

Renormalization group approach to graphene bilayers

L. Delzescaux¹ and D. Mouhanna^{1,*}

¹ Sorbonne Université, CNRS, Laboratoire de Physique Théorique de la Matière Condensée, LPTMC, 75005 Paris, France

We investigate the effects of thermal fluctuations in graphene bilayers by means of a nonperturbative renormalization group (NPRG) approach, following the pioneering work of Mauri *et al.* [Phys. Rev. B **102**, 165421 (2020)] based on a self-consistent screening approximation (SCSA). We consider a model of two continuum polymerized membranes, separated by a distance ℓ , in their flat phase, coupled by interlayer shear, compression/dilatation and elastic terms. Within a controlled truncation of the effective average action, we retain only the contributions that generate a pronounced crossover of the effective bending rigidity along the renormalization group flow between two regimes: at high running scale k , the rigidity is dominated by the in-plane elastic properties, with $\kappa_{\text{eff}} \sim \ell^2(\lambda + 2\mu)/2$, whereas at low k it is controlled by the bending rigidity of two independent monolayers, $\kappa_{\text{eff}} \sim 2\kappa$. This crossover is reminiscent of that observed by Mauri *et al.* as a function of the wavevector scale q , but here it is obtained within a renormalization group framework. This has several advantages. First, although approximations are performed, the NPRG approach allows one, in principle, to take into account all nonlinearities present in the elastic theory, in contrast to the SCSA treatment which requires, already at the formal level, significant simplifications. Second, it demonstrates that the bilayer problem can be treated as a straightforward extension of the monolayer case, with flow equations that keep the same structure and differ only by bilayer-specific adjustments. Third, unlike the SCSA, the NPRG framework admits a controlled, systematically improvable, hierarchy of approximations.

I. INTRODUCTION

Since its isolation in 2004, graphene [1, 2] has attracted immense interest owing to its outstanding physical properties, which set it apart from most other materials. Its key features include extremely high electrical conductivity, arising from the large mobility of its charge carriers, exceptional thermal conductivity, and mechanical strength far exceeding that of steel while remaining extremely lightweight (see e.g., Refs. [3, 4]). Moreover, despite its finite electronic density, graphene is almost perfectly transparent. Its unique electronic structure, with Dirac fermions behaving as relativistic quasiparticles, also enables the exploration of unconventional quantum regimes [3, 5].

While graphene monolayers have been extensively studied, interest in graphene bilayers has grown steadily in recent years (see, e.g., Refs. [6–8]). Composed of two stacked graphene sheets, bilayers exhibit tunable electronic properties that distinguish them from monolayer graphene (see, e.g., Refs. [9, 10]). These structures offer novel possibilities, including band-gap modulation under a perpendicular electric field, as well as the emergence of exotic phases such as superconductivity and Mott insulating states in specific configurations, notably in twisted bilayer graphene (see, e.g., Refs. [7, 11–13]).

Here we focus on the elastic properties of these systems, which, as is well known from the study of monolayers, already provide an extremely fruitful interplay between two-dimensional fluctuating geometry and thermal fluctuations [14]. We therefore now turn to the modeling of the elasto-mechanical properties of graphene. At long distances, graphene can be described as a two-dimensional polymerized membrane embedded in three-dimensional space (see, e.g.,

Refs. [15–17]), where out-of-plane flexural fluctuations, \mathbf{h} , are coupled to in-plane elastic phonon fluctuations, \mathbf{u} . Within a Gaussian approximation, integrating out the phonon degrees of freedom generates an effective long-range interaction between flexural modes, which plays a crucial role in stabilizing long-range order [18–20], in spite of the Mermin–Wagner theorem [21, 22]. This mechanism underlies, in particular, the remarkable mechanical stability of graphene.

Moreover, it has been shown that in the ordered, flat phase of two-dimensional polymerized membranes, which is controlled from the renormalization group (RG) point of view by an infrared fixed point [23, 24], one observes power-law behaviours for both the phonon–phonon and flexuron–flexuron correlation functions [19, 23, 25, 26]:

$$G_{uu}(q) \underset{\mathbf{q} \rightarrow 0}{\sim} q^{-(4-2\eta)} \quad G_{hh}(q) \underset{\mathbf{q} \rightarrow 0}{\sim} q^{-(4-\eta)}, \quad (1)$$

where η is the unique and emblematic exponent characterizing this infrared fixed point. It also governs the scale dependence of the renormalized bending rigidity:

$$\kappa_R(q) \sim q^{-\eta}. \quad (2)$$

The exponent η has been estimated by various analytical and numerical techniques. Self-consistent screening approximation (SCSA) calculations [27–30] already predicted a strong stiffening of $\kappa_R(q)$, with $\eta \simeq 0.821$ at leading order and $\eta \simeq 0.789$ at next-to-leading order [31]. High-precision Monte Carlo and molecular dynamics simulations [32–34] later reported values in the range $\eta \simeq 0.72\text{--}0.81$, e.g. $\eta = 0.795(10)$ [34], confirming both the existence of non-trivial anomalous elasticity and the importance of corrections to scaling. More recently, high-order field-theoretic RG [35–39] and nonperturbative RG (NPRG) approaches [40–43] have yielded estimates clustered in the range $\eta \approx 0.8\text{--}0.9$. In particular, three- and four-loop results and NPRG analyses are mutually consistent, reinforcing the picture of a universal, strongly renormalized flat phase. These last

* mouhanna@lptmc.jussieu.fr

values are also in very close agreement with Monte Carlo and molecular-dynamics simulations using realistic interaction potentials for graphene [44].

Regarding graphene bilayers, let us first discuss the experimental situation; see Ref. [45] for an earlier overview. The effective bending rigidity of suspended graphene membranes and few-layer stacks has been extracted from nanoindentation and snap-through measurements on buckled drums. In particular, Lindahl *et al.* [46] have reported a room-temperature bending rigidity of $\kappa \simeq 35.5^{+20}_{-15}$ eV for bilayer graphene, significantly larger than typical monolayer estimates of order 1-2 eV, and, more generally, a marked increase of apparent stiffness with layer number. More recent modal-analysis experiments on monolayer graphene and helium-atom-scattering measurements on AB-stacked bilayer graphene have shown that the effective bending rigidity depends sensitively on both temperature and system size and, in the bilayer case, can exceed significantly twice the microscopic monolayer value, in agreement with the idea of a thermally renormalized $\kappa_{\text{eff}}(q, T)$ [47, 48].

On the numerical side, atomistic simulations have provided a complementary microscopic picture. Monte Carlo simulations of bilayer graphene by Zakharchenko *et al.* [28] have shown that the bending rigidity of a free bilayer is approximately twice that of a monolayer, and that there is a crossover from correlated to uncorrelated out-of-plane fluctuations of the two layers at a wave vector of order $q \sim 3 \text{ nm}^{-1}$, highlighting the role of interlayer coupling in the long-wavelength flexural response. More recently, Herrero and Ramírez [49] have carried out extensive molecular-dynamics simulations of bilayer graphene over a wide temperature range, showing that the in-plane compression modulus of the bilayer is larger than that of a monolayer but decreases with increasing temperature, and that the onset of mechanical instability under in-plane compression is controlled by a size-dependent spinodal pressure and pronounced finite-size effects in the out-of-plane fluctuations and elastic constants. Their analysis of height fluctuations also indicates that out-of-plane corrugations are significantly reduced in the bilayer compared to a monolayer of the same lateral size and temperature, consistently with an enhanced effective bending rigidity. In addition, molecular-dynamics and Monte Carlo simulations of few-layer graphene and related van der Waals stacks reveal a rich thickness dependence of the flexural response, including a strong softening of the apparent bending stiffness due to interlayer shear and slip at large bending angles [50, 51]. Taken together, these studies indicate that the mechanical response of bilayer and multilayer membranes is governed by a nontrivial interplay between in-plane elasticity, interlayer coupling, and thermal fluctuations, and call for a theoretical framework capable of treating these ingredients on an equal footing and across scales.

On the theoretical side, only a few investigations have been carried out. A long-distance elastic action incorporating interlayer interactions was first proposed by de Andrés *et al.* in Ref. [52], and later derived more systematically by Mauri *et al.* in Ref. [45].

The latter authors studied this model within a SCSA framework and identified a crossover for the (bare) bending rigidity between two regimes: at short distances, a behaviour controlled by the in-plane elastic properties, and at long distances, a behaviour dominated by the bending rigidity of the two layers. This specific rigidity crossover comes in addition to the usual one already known for monolayers, namely the crossover between a quasi-harmonic regime at short distances and a strong-coupling, anharmonic regime at long distances, induced by nonlinear interactions between flexural modes.

However, the approach developed and used by Mauri *et al.* [45] disregards contributions that could play a significant role, in particular the nonlinearities associated with fluctuations of the relative coordinates of the two monolayers. This simplification is the price to pay to construct an effective flexural-mode theory formally analogous to that used for graphene monolayers, which moreover involves a wavevector-dependent bare bending rigidity. As a consequence, the resulting SCSA equations become rather cumbersome and offer limited physical transparency. Finally, at least for membranes, it has been argued that the SCSA, in its current formulation, cannot be systematically improved beyond the leading-order approximation [31].

In this work, we extend the nonperturbative renormalization group (NPRG) framework developed for monolayers to symmetric bilayer crystalline membranes [40–42]. We formulate the problem directly in terms of the average position field and the relative displacement field, which allows us to preserve full rotational invariance and, in principle, to retain all nonlinearities of the elastic theory. Within a simple truncation of the average effective action, the flow equations keep the same structure as in the monolayer case, and the bilayer nature enters only through a modified flexural propagator for the mean-height mode. This enables us to compute the scale dependence of the effective bending rigidity of a bilayer, $\kappa_{\text{eff}}(q)$, and to recover explicitly the full crossover from the short-scale regime $\kappa_{\text{eff}}(q) \sim \ell^2(\lambda + 2\mu)/2$ to the large-scale regime $\kappa_{\text{eff}}(q) \sim 2\kappa$. Our results thus provide a controlled, systematically improvable, symmetry-preserving alternative to SCSA-type treatments of bilayers [45] and clarify in which sense the bilayer problem can be viewed as a straightforward extension of the monolayer case.

Finally, we emphasize that in the present article we focus primarily on the methodological and conceptual aspects of the approach, rather than on a precise quantitative analysis, which will be addressed in a more systematic study.

The structure of this article is as follows. In Sec. II A, we recall the long-distance elastic action relevant for describing a single polymerized membrane in its ordered, flat phase. In Sec. II B, we extend this description to the case of membrane bilayers. Section III A provides a brief overview of the renormalization group procedure based on the Wetterich equation, which allows us to derive nonperturbative flow equations. In Sec. III B, we revisit the RG treatment of a single-layer membrane, before deriving in Sec. III

C the corresponding flow equations for the membrane bilayer system. Finally, in Sec. IV, we present and discuss the physical implications of our results.

II. ELASTIC ACTIONS FOR POLYMERIZED MEMBRANES

A. Membrane monolayers

1. Action

Here we introduce the action relevant for a study of a single membrane. We consider a two-dimensional membrane embedded in a three-dimensional Euclidean space. Each point of the membrane is labeled by internal coordinates $\mathbf{x} \in \mathbb{R}^2$, and its position in embedding space is given by the mapping $\mathbf{x} \mapsto \mathbf{R}(\mathbf{x})$, where \mathbf{R} is a vector field in \mathbb{R}^3 . The energy of a polymerized membrane can be constructed as an expansion in terms of the tangent fields $\partial_\alpha \mathbf{R}$, $\alpha = 1, 2$, and their derivatives. The corresponding long-distance elastic action reads [18, 53]

$$S[\mathbf{R}] = \int d^2x \left\{ \frac{\kappa}{2} (\partial_\alpha^2 \mathbf{R})^2 + \frac{t}{2} (\partial_\alpha \mathbf{R})^2 + \frac{\lambda}{8} (\partial_\alpha \mathbf{R} \cdot \partial_\alpha \mathbf{R})^2 + \frac{\mu}{4} (\partial_\alpha \mathbf{R} \cdot \partial_\beta \mathbf{R})^2 \right\}. \quad (3)$$

In Eq. (3), Greek indices run from 1 to 2 and repeated indices are summed over. The action Eq. (3) contains four contributions: the first term describes the bending energy, with bending rigidity κ , while the second term represents an effective surface tension, with tension parameter t . The last two terms account for stretching and shear elastic energies arising from the fixed connectivity, and are characterized by the two Lamé coefficients λ and μ . Mechanical stability requires that κ , μ , and the bulk modulus $B = \lambda + \mu$ are all positive. Note that in Eq. (3) the temperature has been absorbed into the definition of the field and of the coupling constants.

2. Phase transition and phase structure

Let us examine action Eq.(3) at the mean-field level, varying the parameter t . When $t > 0$, the minimum of Eq. (3) corresponds to a vanishing average value of the order parameter, i.e. $\langle \partial_\alpha \mathbf{R}_0 \rangle = \mathbf{0}$, which characterizes a crumpled phase. In contrast, when $t < 0$, the minimum of Eq. (3) is reached for a configuration

$$\langle \mathbf{R}_0 \rangle = \zeta x_\alpha \mathbf{e}_\alpha, \quad (4)$$

where $\zeta = \sqrt{-t/(\lambda + \mu)}$ and $\{\mathbf{e}_\alpha\}$ is an orthonormal basis defining the orientation of the flat phase in the embedding space. The parameter ζ , with $0 < \zeta < 1$, sets the magnitude of the order parameter components, $\langle \partial_\alpha \mathbf{R} \rangle = \zeta \mathbf{e}_\alpha$ for $\alpha = 1, 2$, and thus quantifies how much the membrane is stretched. The point $t = 0$ therefore corresponds to a phase transition between a high-temperature crumpled phase and a low-

temperature flat phase with long-range orientational order [53, 54].

3. Perturbative and nonperturbative approaches

In order to study the flat phase within the NRG approach, it is convenient to rewrite Eq.(3) in terms of the extension parameter ζ . One gets:

$$S[\mathbf{R}] = \int d^2x \left\{ \frac{\kappa}{2} (\partial_\alpha^2 \mathbf{R})^2 + \frac{\lambda}{8} (\partial_\alpha \mathbf{R} \cdot \partial_\alpha \mathbf{R} - \zeta^2 \delta_{\alpha\alpha})^2 + \frac{\mu}{4} (\partial_\alpha \mathbf{R} \cdot \partial_\beta \mathbf{R} - \zeta^2 \delta_{\alpha\beta})^2 \right\} \quad (5)$$

which should be understood as the leading order of an expansion around the flat phase configuration Eq. (4). One can express Eq. (5) more synthetically in terms of the strain tensor $u_{\alpha\beta} = 1/2(\partial_\alpha \mathbf{R} \cdot \partial_\beta \mathbf{R} - \partial_\alpha \mathbf{R}_0 \cdot \partial_\beta \mathbf{R}_0)$ that measures the deformations with respect to the flat phase configuration Eq. (4):

$$S[\mathbf{R}] = \int d^2x \left\{ \frac{\kappa}{2} (\partial_\alpha^2 \mathbf{R})^2 + \frac{\lambda}{2} u_{\alpha\alpha}^2 + \mu u_{\alpha\beta}^2 \right\}. \quad (6)$$

A fundamental point is that the actions Eqs. (3), (5) and (6) are formulated entirely in terms of the position field \mathbf{R} . Moreover, although we focus on the flat phase, we deliberately refrain from decomposing \mathbf{R} into in-plane phonon and out-of-plane flexural (flexuron) modes around the flat-phase configuration \mathbf{R}_0 , $\mathbf{R}(\mathbf{x}) = \langle \mathbf{R}_0(\mathbf{x}) \rangle + \mathbf{u}(\mathbf{x}) + \mathbf{h}(\mathbf{x})$. Indeed, such a decomposition is usually accompanied by the additional approximations [18, 19, 23]

$$\begin{cases} (\partial_\alpha^2 \mathbf{u})^2 \simeq 0, \\ u_{\alpha\beta} \simeq \frac{1}{2} (\partial_\alpha u_\beta + \partial_\beta u_\alpha + \partial_\alpha \mathbf{h} \cdot \partial_\beta \mathbf{h}) + \mathcal{O}((\partial u)^2), \end{cases} \quad (7)$$

which are well suited either for a *perturbative* analysis of fluctuations around the flat phase [23, 25, 26, 35–39], or for a SCSA treatment based on an effective field theory formulated solely in terms of the flexural fields \mathbf{h} [15, 27–30, 55]. By contrast, the actions Eqs. (3), (5) and (6), which display explicit and full rotational invariance, allow one to investigate within a single framework both the crumpled-to-flat transition and the flat phase of membranes in a genuinely nonperturbative way [40–42], i.e. without relying on expansions in the elastic couplings λ and μ or in any of the usual perturbative parameters (inverse dimension $1/d$, temperature T , etc.).

B. Membrane bilayers

1. Flat phase

We now turn to the field theoretical description of membrane bilayers composed of two monolayers 1 and 2 separated by a distance ℓ . In doing so, we follow the constructions of Refs. [45, 52]. Each monolayer is

described by a free action $S[\mathbf{R}_i]$, $i = 1, 2$, where $S[\mathbf{R}]$ is given by Eqs. (3), (5) or (6), and \mathbf{R}_i ($i = 1, 2$) are the position fields of the two membranes, see Fig. 1.

In the flat phase, the system is characterized by the following ground state:

$$\begin{cases} \langle \mathbf{R}_1 \rangle = \zeta x_\alpha \mathbf{e}_\alpha + \frac{\ell}{2} \mathbf{n}, \\ \langle \mathbf{R}_2 \rangle = \zeta x_\alpha \mathbf{e}_\alpha - \frac{\ell}{2} \mathbf{n} \end{cases} \quad (8)$$

with \mathbf{n} the normal to the monolayers

It is convenient to parametrize the interaction in terms of the mean (center-of-mass) position, $\mathbf{R} = \frac{1}{2}(\mathbf{R}_1 + \mathbf{R}_2)$, and the relative position, $\mathbf{S} = \mathbf{R}_1 - \mathbf{R}_2$. In terms of these fields, the flat-phase configuration is described by

$$\begin{cases} \langle \mathbf{R}_0 \rangle = \zeta x_\alpha \mathbf{e}_\alpha, \\ \langle \mathbf{S}_0 \rangle = \ell \mathbf{n} \end{cases} \quad (9)$$

that generalize Eq.(4).

2. Symmetries

Under a simultaneous translation $\mathbf{R}_{1,2} \rightarrow \mathbf{R}_{1,2} + \mathbf{C}$, with \mathbf{C} an arbitrary three-dimensional vector, the center-of-mass coordinate $\mathbf{R} = \frac{1}{2}(\mathbf{R}_1 + \mathbf{R}_2)$ transforms as $\mathbf{R} \rightarrow \mathbf{R} + \mathbf{C}$, while the relative coordinate $\mathbf{S} = \mathbf{R}_1 - \mathbf{R}_2$ remains invariant. Translational invariance therefore constrains the effective theory so that \mathbf{R} can only appear through its derivatives, $\partial_\alpha \mathbf{R}$. The corresponding excitations are Goldstone modes associated with the spontaneous breaking of translational symmetry by the presence of the membrane, and are consequently massless. In contrast, because \mathbf{S} is invariant under global translations, this symmetry does not restrict the form of local potentials $V(\mathbf{S})$ or couplings such as $(\mathbf{S}^2 - \ell^2) u_{\alpha\alpha}$ that mix \mathbf{S} with the in-plane strain of the center-of-mass field \mathbf{R} , see below. Fluctuations in \mathbf{S} describe internal degrees of freedom, such as local variations of thickness or relative tilt between the two monolayers, and acquire a finite mass.

3. Action

The explicit form of the interaction $S_I[\mathbf{R}, \mathbf{S}]$ between the two membranes can be obtained from the above symmetry considerations, together with the requirement that, in order to preserve rotational invariance in the embedding space, it must be built only from scalar combinations of $\{\partial_\alpha \mathbf{R}\}$ and \mathbf{S} . In addition, it should describe small fluctuations around the configuration Eq. (9). Accordingly, it can depend on the in-plane strain tensor $u_{\alpha\beta}$, the interlayer shear $\mathbf{S} \cdot \partial_\alpha \mathbf{R}$, and fluctuations of the interlayer distance, encoded in the term $\mathbf{S}^2 - \ell^2$. The action compatible

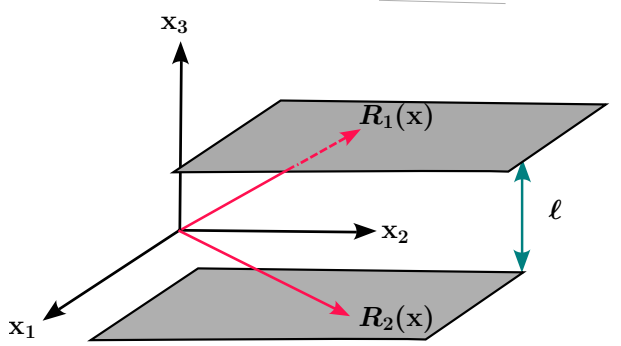


FIG. 1. Bilayer model: two coupled membranes, separated by a distance ℓ . A point on membrane 1 (respectively, membrane 2) is parameterized by the position vector $\mathbf{R}_1(\mathbf{x})$ (respectively, $\mathbf{R}_2(\mathbf{x})$).

with all these symmetries is given by [45]

$$S_I[\mathbf{R}, \mathbf{S}] = \int d^2x \left\{ \frac{g_1}{8\ell^4} (\mathbf{S}^2 - \ell^2)^2 + \frac{g_2}{2\ell^2} (\mathbf{S} \cdot \partial_\alpha \mathbf{R})^2 + \frac{g_3}{4\ell^2} (\mathbf{S}^2 - \ell^2) u_{\alpha\alpha} \right\}. \quad (10)$$

Note that here we have neglected anisotropic terms which are relevant for realistic graphene-based materials but are expected to be subdominant compared to the contributions retained in Eq. (10) (see Ref. [45]). The interaction action $S_I[\mathbf{R}, \mathbf{S}]$ contains three terms. The first one is a restoring potential that drives \mathbf{S}^2 towards ℓ^2 . The second term is a tilt (director-tangent) coupling: it penalizes the projection of \mathbf{S} onto the local tangent directions $\partial_\alpha \mathbf{R}$, and thus suppresses relative tilt of the interlayer director \mathbf{S} with respect to the membrane's tangent frame, stabilizing the alignment of \mathbf{S} along the local normal. The last term is a volume-area coupling: it couples thickness fluctuations to areal strain, so that stretching ($u_{\alpha\alpha} > 0$) favors thinning ($\mathbf{S}^2 < \ell^2$), while compression ($u_{\alpha\alpha} < 0$) favors thickening ($\mathbf{S}^2 > \ell^2$), thereby encoding approximate local volume conservation.

The whole action, given by $S[\mathbf{R}, \mathbf{S}] = S[\mathbf{R}_1] + S[\mathbf{R}_2] + S_I[\mathbf{R}, \mathbf{S}]$ reads, in terms of the fields \mathbf{R} and \mathbf{S} [45]:

$$\begin{aligned} S[\mathbf{R}, \mathbf{S}] = & \int d^2x \left\{ \frac{\kappa}{2} \left(2(\partial^2 \mathbf{R})^2 + \frac{1}{2} (\partial^2 \mathbf{S})^2 \right) + \lambda u_{\alpha\alpha}^2 \right. \\ & + 2\mu u_{\alpha\beta}^2 + \frac{\lambda}{4} (\partial_\alpha \mathbf{R} \cdot \partial_\alpha \mathbf{S})^2 + \frac{\mu}{4} (\partial_\alpha \mathbf{S} \cdot \partial_\beta \mathbf{R})^2 \\ & + \frac{\lambda}{64} (\partial_\alpha \mathbf{S} \cdot \partial_\alpha \mathbf{S})^2 + \frac{\mu}{32} (\partial_\alpha \mathbf{S} \cdot \partial_\beta \mathbf{S})^2 + \frac{\lambda}{4} u_{\alpha\alpha} \partial_\beta \mathbf{S} \cdot \partial_\beta \mathbf{S} \\ & + \frac{\mu}{2} u_{\alpha\beta} \partial_\alpha \mathbf{S} \cdot \partial_\beta \mathbf{S} + \frac{\mu}{4} (\partial_\alpha \mathbf{R} \cdot \partial_\beta \mathbf{S}) (\partial_\alpha \mathbf{S} \cdot \partial_\beta \mathbf{R}) \\ & \left. + \frac{g_1}{8\ell^4} (\mathbf{S}^2 - \ell^2)^2 + \frac{g_2}{2\ell^2} (\mathbf{S} \cdot \partial_\alpha \mathbf{R})^2 + \frac{g_3}{4\ell^2} (\mathbf{S}^2 - \ell^2) u_{\alpha\alpha} \right\}. \end{aligned} \quad (11)$$

An important point to notice is that the coupling constants in front of the elastic contributions $u_{\alpha\alpha}^2$ and $u_{\alpha\beta}^2$ can be deduced from those entering in action Eq. (6) by the rescaling: $\lambda \rightarrow 2\lambda$ and $\mu \rightarrow 2\mu$.

Following and drawing on the works of de Andrés *et al.* [52] and Mauri *et al.* [45], we will focus, among the three interaction terms, on the one responsible for the rigidity crossover, namely the coupling proportional to g_2 that we take very large. Moreover we will take the limit $g_1 \rightarrow \infty$, which fixes the interlayer separation to $|\mathbf{S}| = \ell$. In this limit, the term proportional to g_3 does not contribute, since it is multiplied by $\mathbf{S}^2 - \ell^2$.

III. NONPERTURBATIVE RENORMALIZATION GROUP APPROACH TO POLYMERIZED MEMBRANES

A. Methodology

We now present the NPRG method used to investigate graphene bilayers. It relies on the concept of a running Gibbs free energy – or effective average action [56–61]. Fundamentally, it is based on the Wilson-Kadanoff block-spin idea [62], in which one integrates out short-distance degrees of freedom in the partition function in order to obtain an effective Hamiltonian or action for the long-distance modes. It was realized in the 90's [63, 64], however, that it is more convenient, both conceptually and computationally, to work with a more physical quantity than the Hamiltonian or action, namely the Gibbs free energy Γ . One therefore introduces a running Gibbs free energy – or effective average action – Γ_k , where k is a running wavevector scale in the block-spin procedure. By construction, Γ_k is the Gibbs free energy in which only fluctuations with wavevectors $q \geq k$ have been integrated out. As a consequence, at the microscopic (lattice) scale $k = \Lambda$ (often formally taken to infinity), one has $\Gamma_{k=\Lambda} = S$, where S is the bare action or Hamiltonian, since no fluctuations have been integrated out. Conversely, at the macroscopic scale $k = 0$, Γ_k coincides with the usual Gibbs free energy Γ :

$$\begin{cases} \Gamma_{k=\Lambda} = S, \\ \Gamma_{k=0} = \Gamma, \end{cases} \quad (12)$$

and Γ_k with $0 \leq k \leq \Lambda$ interpolates smoothly between these two limits.

We now construct the running Gibbs free energy for the field theory with a single order parameter \mathbf{R} , which is relevant for a monolayer, and postpone the discussion of the bilayer case to later.

First, one has to separate the low-wavevector modes from the high-wavevector ones in order to integrate out the latter. To achieve this separation, we introduce a k -dependent quadratic “mass” term

$$\Delta S_k[\mathbf{R}] = \frac{1}{2} \int_{\mathbf{q}} R_{k,ij}(\mathbf{q}) R_i(\mathbf{q}) R_j(-\mathbf{q}), \quad (13)$$

where $R_{k,ij}(\mathbf{q})$ ($i, j = 1, \dots, 3$) is a \mathbf{q} -dependent cut-off function, which is very often taken to be diagonal, $R_{k,ij}(\mathbf{q}) = R_k(\mathbf{q}) \delta_{ij}$. The partition function in the

presence of a source $\mathbf{J}(\mathbf{q})$ then reads

$$Z_k[\mathbf{J}] = \int \mathcal{D}\mathbf{R} \exp \left[-S[\mathbf{R}] - \Delta S_k[\mathbf{R}] + \int_{\mathbf{q}} \mathbf{J}(\mathbf{q}) \cdot \mathbf{R}(-\mathbf{q}) \right], \quad (14)$$

with $\int_{\mathbf{q}} \equiv \int d^2\mathbf{q}/(2\pi)^2$. The role of the term Eq. (13) is to suppress low-wavevector modes so that only high-wavevector modes are effectively integrated out in Eq. (14). In order to implement this program and ensure that Γ_k satisfies the limits Eq. (12), the cut-off function $R_k(\mathbf{q})$ must satisfy the following properties:

1) At fixed k :

- $R_k(\mathbf{q}) \sim k^\alpha$ with $\alpha > 0$ when $|\mathbf{q}| \ll k$: low-wavevector modes acquire an effective “mass” of order k^α and thus effectively decouple.
- $R_k(\mathbf{q}) \rightarrow 0$ when $|\mathbf{q}| \gg k$: high-wavevector modes are essentially unaffected by the regulator term.

2) At fixed q :

- $R_k(\mathbf{q}) \rightarrow 0$ when $k \rightarrow 0$: the regulator term vanishes when all fluctuations have been integrated out, so that the mass term no longer plays any role.
- $R_k(\mathbf{q}) \rightarrow \Lambda^\alpha$ when $k \rightarrow \Lambda$ (with Λ generally taken infinite): at the lattice scale, $R_k(\mathbf{q})$ acts as a very large mass for all modes. They are effectively “frozen” and do not contribute to the functional integral Eq. (14).

A typical cut-off function satisfying these properties is the exponential regulator [58]:

$$R_k(\mathbf{q}) = \frac{Z_k |\mathbf{q}|^\alpha}{\exp(|\mathbf{q}|^\alpha/k^\alpha) - 1}, \quad (15)$$

where Z_k is a field renormalization factor, see below. This function is illustrated in Fig. 2. A very practical and commonly used choice is the Litim (or Θ) cut-off [65],

$$R_k(\mathbf{q}) = Z_k (k^\alpha - |\mathbf{q}|^\alpha) \Theta(k^\alpha - |\mathbf{q}|^\alpha), \quad (16)$$

where Θ denotes the Heaviside step function.

We now define the running Gibbs free energy Γ_k as a slightly modified Legendre transform of the Helmholtz free energy:

$$\Gamma_k[\mathbf{r}] = -W_k[\mathbf{J}] + \int_{\mathbf{q}} \mathbf{J}(\mathbf{q}) \cdot \mathbf{r}(-\mathbf{q}) - \Delta S_k[\mathbf{r}], \quad (17)$$

with $W_k[\mathbf{J}] = \log Z_k[\mathbf{J}]$, where we have set $k_B T = 1$, and where \mathbf{r} is the expectation value of the microscopic field \mathbf{R} in the presence of the source \mathbf{J} :

$$r_i = \langle R_i \rangle = \frac{\delta W_k[\mathbf{J}]}{\delta J_i}. \quad (18)$$

With this definition, together with the properties of the cut-off function $R_k(\mathbf{q})$ specified above, it is

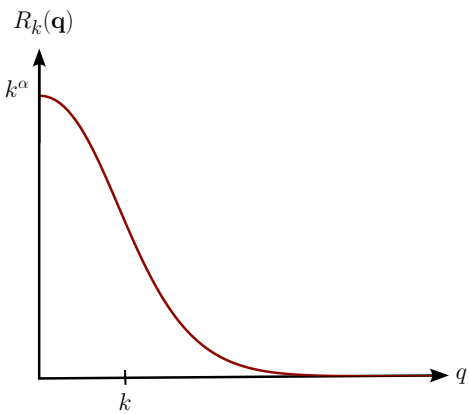


FIG. 2. A typical shape of the cut-off function $R_k(\mathbf{q})$.

straightforward to check that Γ_k satisfies the limits Eq. (12).

The running Gibbs free energy – or effective average action – Γ_k follows an exact equation, namely the Wetterich equation [63]:

$$\begin{aligned} \partial_t \Gamma_k[\mathbf{r}] &= \frac{1}{2} \int_{\mathbf{q}} \partial_t R_{k,ij}(\mathbf{q}) \left(\Gamma_{k,ji}^{(2)}[\mathbf{r}; \mathbf{q}, -\mathbf{q}] + R_{k,ji}(\mathbf{q}) \right)^{-1} \\ &\equiv \frac{1}{2} \text{Tr} \left[\partial_t R_k \left(\Gamma_k^{(2)} + R_k \right)^{-1} \right] \end{aligned} \quad (19)$$

where the trace is performed on both discrete and continuum indices. In Eq. (19) one has defined a RG “time” $t = \ln k/\Lambda$. A practical expression is given by:

$$\partial_t \Gamma_k[\mathbf{r}] = \frac{1}{2} \widehat{\partial}_t \text{Tr} \ln \left[\Gamma_k^{(2)} + R_k \right] \quad (20)$$

with $\widehat{\partial}_t \equiv \partial_t R_k(\mathbf{q}) \partial_{R_k(\mathbf{q})}$.

In Eqs. (19) and (20), $\Gamma_{k,ij}^{(2)}[\mathbf{r}; \mathbf{q}, -\mathbf{q}]$ is the inverse propagator, *i.e.* the second derivative of Γ_k with respect to the order parameter field \mathbf{r} :

$$\Gamma_{k,ij}^{(2)}[\mathbf{r}; \mathbf{q}, -\mathbf{q}] = \frac{\delta^2 \Gamma_k[\mathbf{r}]}{\delta r_i(\mathbf{q}) \delta r_j(-\mathbf{q})} \quad (21)$$

considered in a generic field configuration.

Eqs. (19) and (20) govern the evolution of Γ_k as k is lowered, *i.e.* as fluctuations with lower and lower wavevectors are successively included. In these equations, the cut-off function R_k appears both in the numerator of the integrand, through $\partial_t R_k$, and in the denominator as a “mass term” in the propagator. In the former case, combined with the generic shape of the regulated propagator (see Fig. 2), this ensures that only modes with wavevectors in a shell around k contribute effectively to the RG flow, in accordance with the Wilsonian picture. In particular, R_k controls the ultraviolet (UV) sector. In the latter case, R_k acts as an infrared (IR) regulator, which guarantees that even at criticality any singular behaviour is shifted to vanishing wavevector in the limit $k \rightarrow 0$. This mechanism works provided the exponent α in k^α is chosen appropriately: for scalar theories with $O(N)$ symmetry and a standard kinetic term of order ∂^2 , one takes

$\alpha = 2$, whereas for crystalline membranes, whose kinetic term is of order ∂^4 , one chooses $\alpha = 4$ [40]. With this choice, one can safely investigate any phase or phase transition by taking the limit $k \rightarrow 0$.

Let us comment on Eq. (19) in more detail. 1) First, it is exact. As such, it can in principle be used to investigate both perturbative excitations (such as magnons, phonons, or flexurons) and genuinely non-perturbative excitations (such as topological or bound states). 2) It involves Γ_k which, besides being a directly physical quantity, is the generating functional of one-particle-irreducible (1PI) vertices, and therefore provides a direct link to standard perturbative computations. 3) It has a one-loop structure, in sharp contrast with systematic loop expansions. This is possible because the propagator entering Eq. (19) carries the *full* field dependence, whereas in perturbation theory one usually deals with a propagator evaluated at vanishing order parameter.

As a consequence, for any generic theory, *e.g.* a scalar ϕ^4 theory,

$$\Gamma_k[\phi] = \int d^D \mathbf{x} \left\{ \frac{1}{2} (\partial\phi)^2 + \frac{1}{2} m^2 \phi^2 + \frac{g}{4!} \phi^4 + \dots \right\}, \quad (22)$$

the propagator evaluated at a nonvanishing uniform field $\phi = \phi_0$, $G_k[\phi_0, \mathbf{q}]$, exhibits a nontrivial dependence on the coupling constant g :

$$G_k[\phi_0, \mathbf{q}] = \left(\Gamma_k^{(2)}[\phi; \mathbf{q}, -\mathbf{q}] \Big|_{\phi=\phi_0} \right)^{-1} = \frac{1}{\mathbf{q}^2 + m^2 + \frac{g}{2} \phi_0^2 + \dots} \quad (23)$$

Although exact, the running Gibbs free energy Γ_k entering Eq. (19) must be approximated (truncated) in practice. A very successful approximation consists in expanding Γ_k in powers of derivatives of the order parameter [57, 58, 61]. This type of expansion relies on two main ingredients. 1) From a technical point of view, it uses the fact that functional derivatives of $\Gamma_k[\mathbf{r}]$ with respect to the field r_i are smooth functions of the wavevectors and can be expanded in powers of p_i/k^2 or p_i/m , where m is a typical wavevector also (improperly) called “mass” scale [61]. This property is guaranteed by the infrared finiteness of the Wetterich equation. 2) From a physical point of view, it assumes that the essential physics is governed by long-distance (thus low-derivative) modes. This is typically the case when the running Gibbs free energy is parametrized in terms of the relevant low-wavevector degrees of freedom, which do not form bound states.

This derivative expansion is often accompanied by an expansion in powers of the field, *see* Refs. [58, 61] for reviews, as long as the physics is not controlled by a nonanalytic dependence on the order parameter. A notable exception arises in the presence of strong disorder, *e.g.* in the random-field Ising model, where an infinite number of operators become marginal at the upper or lower critical dimension, *see* Ref. [66] for a review.

The major advantage of these combined approximations, when they are physically justified, is that the

functional equation Eq. (19) is converted into a closed set of differential equations for the coupling constants parametrizing the running Gibbs free energy Γ_k . This greatly simplifies the calculations while preserving the nonperturbative content of the flow, as is apparent from Eq. (23). In the case of membrane monolayers, such approximations have made it possible to treat, within a single framework, both the crumpled-to-flat transition and the flat phase of the membrane – which are nonperturbatively related – with good quantitative accuracy [40–42]. However, achieving high precision in general requires extending the ansatz for Γ_k [43].

Membranes in their flat phase represent a particularly singular case in this context. Indeed, it can be shown that all powers of the order parameter higher than $(\partial_\alpha \mathbf{r})^4$ do not contribute to the RG flow in the flat phase. This is because these contributions are all (pseudo-) massive [67]. These terms have squared pseudo-masses of order $(\lambda, \mu) \times \zeta^2$ and thus decouple at low-wavevectors (as detailed in section III B 4). Moreover, Braghin and Hasselmann [41, 42] have demonstrated, using a wavevector-dependent approximation, that high-wavevector and high-order derivative terms do not contribute significantly. Their analysis found an exponent $\eta \sim 0.85$, which is almost indistinguishable from the value obtained within a derivative expansion at leading order ($\eta \sim 0.849$) [40]. As a result, the combined field/field derivative expansion is highly effective for studying the flat phase of membranes.

B. Monolayers

Before turning to the bilayer case, we first recall how the NPRG works for a single membrane (monolayer), which has been studied in a variety of settings, including isotropic, anisotropic, quantum, and disordered cases [40–43, 68–70]. In this case, the running

Gibbs free energy is taken in the form

$$\Gamma_k[\mathbf{r}] = \int d^2x \left\{ \frac{\kappa_k}{2} (\partial_\alpha^2 \mathbf{r})^2 + \frac{\lambda_k}{2} u_{\alpha\alpha}^2 + \mu_k u_{\alpha\beta}^2 \right\}, \quad (24)$$

with

$$u_{\alpha\beta} = \frac{1}{2} (\partial_\alpha \mathbf{r} \cdot \partial_\beta \mathbf{r} - \zeta_k^2 \delta_{\alpha\beta}). \quad (25)$$

In Eqs. (24) and (25), the couplings κ_k , λ_k , μ_k and ζ_k all depend on the running scale k .

It is convenient to redefine the field \mathbf{r} and the couplings in such a way as to absorb κ_k and make explicit the field renormalization factor Z_k . In terms of these rescaled quantities, one obtains

$$\Gamma_k[\mathbf{r}] = \int d^2x \left\{ \frac{Z_k}{2} (\partial_\alpha^2 \mathbf{r})^2 + \frac{\lambda_k}{2} u_{\alpha\alpha}^2 + \mu_k u_{\alpha\beta}^2 \right\}. \quad (26)$$

1. Derivation of the RG flow: general principle

In order to derive the RG equations from the action Eq. (26), one must first define the running couplings unambiguously from Γ_k . Typically, for a generic coupling constant g_k (including λ_k , μ_k or Z_k), one proceeds as follows:

$$g_k = \lim_{\mathbf{p} \rightarrow 0} \frac{1}{a!} \frac{1}{b!} \frac{\partial^a}{\partial (\mathbf{p}^2)^a} \frac{\partial^b}{\partial (p_c^2)^b} \Gamma_{k,ij}^{(2)}[\mathbf{r}; \mathbf{p}, -\mathbf{p}] \Big|_{\mathbf{r}_{0,k}}, \quad (27)$$

for appropriately chosen values of the indices a, b, c, i, j . In Eq. (27), $\mathbf{r}_{0,k}$ denotes the running flat-phase configuration, see Eq. (4), which writes here:

$$\mathbf{r}_{0,k} = \zeta_k x_\alpha \mathbf{e}_\alpha. \quad (28)$$

In order to obtain the corresponding RG flow, one acts on the right-hand side of (27) with the operator ∂_t . This yields

$$\partial_t g_k = \lim_{\mathbf{p} \rightarrow 0} \frac{1}{a!} \frac{1}{b!} \frac{\partial^a}{\partial (\mathbf{p}^2)^a} \frac{\partial^b}{\partial (p_c^2)^b} \left\{ \partial_t \Gamma_{k,ij}^{(2)}[\mathbf{r}; \mathbf{p}, -\mathbf{p}] \Big|_{\mathbf{r}_{0,k}} + \int_{\mathbf{q}} \Gamma_{k,ijl}^{(3)}[\mathbf{r}; \mathbf{p}, -\mathbf{p}, \mathbf{q}] \partial_t r_k^l(\mathbf{q}) \Big|_{\mathbf{r}_{0,k}} \right\} \quad (29)$$

which couples the RG flow of $\Gamma_{k,ij}^{(2)}[\mathbf{r}; \mathbf{p}, -\mathbf{p}]$ to higher functional derivatives of $\Gamma_k[\mathbf{r}]$. The former is obtained

$$\partial_t \Gamma_{k,ij}^{(2)}[\mathbf{r}; \mathbf{p}, -\mathbf{p}] = \frac{1}{2} \widehat{\partial}_t \left\{ \int_{\mathbf{q}} G_{k,ab}[\mathbf{r}, \mathbf{q}] \Gamma_{k,ijba}^{(4)}[\mathbf{r}; \mathbf{p}, -\mathbf{p}, \mathbf{q}, -\mathbf{q}] - \int_{\mathbf{q}} G_{k,ab}[\mathbf{r}, \mathbf{q}] \Gamma_{k,ibc}^{(3)}[\mathbf{r}; \mathbf{p}, -\mathbf{q}, \mathbf{q} - \mathbf{p}] G_{k,cd}[\mathbf{r}, \mathbf{q} - \mathbf{p}] \Gamma_{k,jda}^{(3)}[\mathbf{r}; -\mathbf{p}, \mathbf{q}, \mathbf{p} - \mathbf{q}] \right\}, \quad (30)$$

where $G_{k,ab}[\mathbf{r}, \mathbf{q}]$ is the the (modified) propagator :

$$G_{k,ab}[\mathbf{r}, \mathbf{q}] = [\Gamma_{k,ab}^{(2)}[\mathbf{r}; \mathbf{q}, -\mathbf{q}] + R_{k,ab}(\mathbf{q})]^{-1}. \quad (31)$$

by taking two functional derivatives of the Wetterich equation Eq. (19), which yields

The flow of the minimum $\mathbf{r}_{0,k}$ – or, more precisely, of the extension factor ζ_k – is defined in a slightly

different way. We start from the condition that $\mathbf{r}_{0,k}$ minimizes Γ_k , namely

$$\Gamma_{k,i}^{(1)}[\mathbf{r}; \mathbf{p}] \Big|_{\mathbf{r}_{0,k}} = \frac{\delta \Gamma_k[\mathbf{r}]}{\delta r_i(\mathbf{p})} \Big|_{\mathbf{r}_{0,k}} = 0, \quad (32)$$

with, in Fourier space,

$$\mathbf{r}_{0,k}(\mathbf{p}) = -i \zeta_k \mathbf{e}_\mu \frac{\partial}{\partial p_\mu} \delta(\mathbf{p}). \quad (33)$$

Note, however, that due to translational invariance any configuration of the form Eq. (33), with ζ_k replaced by an arbitrary constant θ_k , would also satisfy Eq. (32). To lift this ambiguity, it is more convenient to define ζ_k through a stationarity condition with respect to the tangent vector of the membrane, namely

$$\frac{\delta \Gamma_k[\mathbf{r}]}{\delta (\partial_\alpha r_i(\mathbf{p}))} \Big|_{\mathbf{r}_{0,k}} = 0. \quad (34)$$

Acting with ∂_t on Eq. (34) then yields

$$\frac{\delta \partial_t \Gamma_k[\mathbf{r}]}{\delta (\partial_\alpha r_i)} \Big|_{\mathbf{r}_{0,k}} + \int_{\mathbf{q}} \frac{\delta^2 \Gamma_k[\mathbf{r}]}{\delta (\partial_\alpha r_i) \delta (\partial_\beta r_j)} \partial_t (\partial_\beta r_j) \Big|_{\mathbf{r}_{0,k}} = 0, \quad (35)$$

where, using the explicit form Eq. (33) of $\mathbf{r}_{0,k}$, the second term is proportional to $\partial_t \zeta_k$, which can therefore be determined explicitly, see below.

As seen from Eq. (30) – which must be evaluated in the flat-phase configuration Eq. (34) – and Eq. (35), the propagator $G_{k,ab}[\mathbf{r}, \mathbf{q}]$ in this configuration plays a central role in controlling the RG flow of all coupling constants. We now give its explicit expression.

2. Propagators and spectrum of excitations

The propagator at the minimum can be obtained by computing the second functional derivative of Γ_k with respect to the fields $r_i(\mathbf{q})$ and $r_j(-\mathbf{q})$ and then evaluating it in the configuration $\mathbf{r}_{0,k}$. One finds [69]:

$$\Gamma_k^{(2)}[\mathbf{r}; \mathbf{q}, -\mathbf{q}] \Big|_{\mathbf{r}_{0,k}} = \begin{pmatrix} \Gamma_{k,p}^{(2)}[\mathbf{r}; \mathbf{q}, -\mathbf{q}] & \mathbf{0}_{2 \times 1} \\ \mathbf{0}_{1 \times 2} & \Gamma_{k,f}^{(2)}[\mathbf{r}; \mathbf{q}, -\mathbf{q}] \end{pmatrix} \Big|_{\mathbf{r}_{0,k}}, \quad (36)$$

where the subscripts p and f refer to the phonon and flexural sectors, respectively. One has

$$\Gamma_{k,p}^{(2)}[\mathbf{r}; \mathbf{q}, -\mathbf{q}] \Big|_{\mathbf{r}_{0,k}} = \begin{pmatrix} Z_k \mathbf{q}^4 + M_1(\mathbf{q}^2) & \zeta_k^2 (\lambda_k + \mu_k) q_1 q_2 \\ \zeta_k^2 (\lambda_k + \mu_k) q_1 q_2 & Z_k \mathbf{q}^4 + M_2(\mathbf{q}^2) \end{pmatrix}, \quad (37)$$

with

$$M_i(\mathbf{q}^2) = \zeta_k^2 (\mu_k \mathbf{q}^2 + (\lambda_k + \mu_k) q_i^2), \quad (38)$$

and

$$\Gamma_{k,f}^{(2)}[\mathbf{r}; \mathbf{q}, -\mathbf{q}] \Big|_{\mathbf{r}_{0,k}} = Z_k \mathbf{q}^4. \quad (39)$$

The inverse, regularized propagator

$$\Gamma_k^{(2)}[\mathbf{r}; \mathbf{q}, -\mathbf{q}] + R_k(\mathbf{q}) \quad (40)$$

at $\mathbf{r}_{0,k}$ can be conveniently rewritten using projectors parallel and transverse to the wavevector \mathbf{q} in the two-dimensional membrane:

$$\begin{cases} P_{ij}^{\parallel}(\mathbf{q}) = \delta_{\alpha i} \delta_{\beta j} \frac{q_\alpha q_\beta}{\mathbf{q}^2}, \\ P_{ij}^{\perp}(\mathbf{q}) = \delta_{\alpha i} \delta_{\alpha j} - \delta_{\alpha i} \delta_{\beta j} \frac{q_\alpha q_\beta}{\mathbf{q}^2}, \end{cases} \quad (41)$$

with

$$P_{ij}^{\parallel}(\mathbf{q}) + P_{ij}^{\perp}(\mathbf{q}) = \delta_{\alpha i} \delta_{\alpha j}, \quad (42)$$

and the flexural projector

$$P_{ij}^f(\mathbf{q}) = \delta_{ij} - \delta_{\alpha i} \delta_{\alpha j}. \quad (43)$$

In terms of these projectors, one obtains

$$\begin{aligned} \Gamma_{k,ij}^{(2)}[\mathbf{r}; \mathbf{q}, -\mathbf{q}] \Big|_{\mathbf{r}_{0,k}} + R_{k,ij}(\mathbf{q}) &= G_{k,1}^{-1}(\mathbf{q}) P_{ij}^{\perp}(\mathbf{q}) \\ &+ G_{k,2}^{-1}(\mathbf{q}) P_{ij}^{\parallel}(\mathbf{q}) + G_{0,k}^{-1}(\mathbf{q}) P_{ij}^f(\mathbf{q}). \end{aligned} \quad (44)$$

The expression Eq. (44) is easily inverted according to the properties $(P^{\parallel})^2 = (P^{\perp})^2 = 1$ and $P^{\parallel} P^{\perp} = 0$ and one gets:

$$\begin{aligned} \left[\Gamma_{k,ij}^{(2)}[\mathbf{r}; \mathbf{q}, -\mathbf{q}] \Big|_{\mathbf{r}_{0,k}} + R_{k,ij}(\mathbf{q}) \right]^{-1} &= G_{k,1}(\mathbf{q}) P_{ij}^{\perp}(\mathbf{q}) \\ &+ G_{k,2}(\mathbf{q}) P_{ij}^{\parallel}(\mathbf{q}) + G_{k,0}(\mathbf{q}) P_{ij}^f(\mathbf{q}). \end{aligned} \quad (45)$$

In Eqs. (44) and (45), $G_{k,1}(\mathbf{q})$, $G_{k,2}(\mathbf{q})$ and $G_{k,0}(\mathbf{q})$ denote the propagators of the various excitations. More precisely, the spectrum consists of:

- one transverse phonon mode with squared pseudo-mass $m_{1,k}^2 = \zeta_k^2 \mu_k$, whose propagator reads

$$G_{k,1}(\mathbf{q}) = \frac{1}{Z_k \mathbf{q}^4 + m_{1,k}^2 \mathbf{q}^2 + R_k(\mathbf{q})}; \quad (46)$$

- one longitudinal phonon mode with squared pseudo-mass $m_{2,k}^2 = \zeta_k^2 (\lambda_k + 2\mu_k)$, with propagator

$$G_{k,2}(\mathbf{q}) = \frac{1}{Z_k \mathbf{q}^4 + m_{2,k}^2 \mathbf{q}^2 + R_k(\mathbf{q})}; \quad (47)$$

- one flexural (flexuron) mode with vanishing pseudo-mass, whose propagator is

$$G_{k,0}(\mathbf{q}) = \frac{1}{Z_k \mathbf{q}^4 + R_k(\mathbf{q})}. \quad (48)$$

3. RG equations

We now derive the RG equations for the various running couplings and for the field renormalization, which are defined as derivatives of $\Gamma_{k,ij}^{(2)}$ with respect to the external wavevector \mathbf{p} . Explicitly, we set

$$\begin{cases} \mu_k = \frac{1}{\zeta_k^2} \lim_{\mathbf{p} \rightarrow 0} \frac{\partial}{\partial \mathbf{p}^2} \Gamma_{k,22}^{(2)}[\mathbf{r}; \mathbf{p}, -\mathbf{p}] \Big|_{\mathbf{r}_{0,k}}, \\ \lambda_k = \frac{1}{\zeta_k^2} \lim_{\mathbf{p} \rightarrow 0} \frac{\partial}{\partial p_2^2} \Gamma_{k,22}^{(2)}[\mathbf{r}; \mathbf{p}, -\mathbf{p}] \Big|_{\mathbf{r}_{0,k}} - \mu_k, \\ Z_k = \lim_{\mathbf{p} \rightarrow 0} \frac{\partial^2}{\partial (\mathbf{p}^2)^2} \Gamma_{k,33}^{(2)}[\mathbf{r}; \mathbf{p}, -\mathbf{p}] \Big|_{\mathbf{r}_{0,k}}, \end{cases} \quad (49)$$

where p_2 denotes the second component of \mathbf{p} .

Taking the RG-time derivative ∂_t of these definitions and using the general flow identity Eq. (29) yields, for μ_k ,

$$\begin{aligned} \partial_t \mu_k = \lim_{\mathbf{p} \rightarrow 0} \frac{\partial}{\partial \mathbf{p}^2} \left[\frac{1}{\zeta_k^2} \partial_t \Gamma_{k,22}^{(2)}[\mathbf{r}; \mathbf{p}, -\mathbf{p}] \right. \\ \left. - \frac{2}{\zeta_k^3} \partial_t \zeta_k \Gamma_{k,22}^{(2)}[\mathbf{r}; \mathbf{p}, -\mathbf{p}] \right. \\ \left. + \frac{1}{\zeta_k^2} \int_{\mathbf{q}} \Gamma_{k,22j}^{(3)}[\mathbf{r}; \mathbf{p}, -\mathbf{p}, \mathbf{q}] \partial_t r_j(\mathbf{q}) \right] \Big|_{\mathbf{r}=\mathbf{r}_{0,k}} \end{aligned} \quad (50)$$

where we have taken into account the k – or t – dependence of the extension parameter ζ_k .

A similar expression holds for λ_k :

$$\begin{aligned} \partial_t \lambda_k = \lim_{\mathbf{p} \rightarrow 0} \frac{\partial}{\partial \mathbf{p}_2^2} \left[\frac{1}{\zeta_k^2} \partial_t \Gamma_{k,22}^{(2)}[\mathbf{r}; \mathbf{p}, -\mathbf{p}] \right. \\ \left. - \frac{2}{\zeta_k^3} \partial_t \zeta_k \Gamma_{k,22}^{(2)}[\mathbf{r}; \mathbf{p}, -\mathbf{p}] \right. \\ \left. + \frac{1}{\zeta_k^2} \int_{\mathbf{q}} \Gamma_{k,22j}^{(3)}[\mathbf{r}; \mathbf{p}, -\mathbf{p}, \mathbf{q}] \partial_t r_j(\mathbf{q}) \right] \Big|_{\mathbf{r}=\mathbf{r}_{0,k}} \\ - \partial_t \mu_k. \end{aligned} \quad (51)$$

Finally, the flow of the field renormalization Z_k can be written as

$$\begin{aligned} \partial_t Z_k = \lim_{\mathbf{p} \rightarrow 0} \frac{\partial^2}{\partial (\mathbf{p}^2)^2} \left[\partial_t \Gamma_{k,33}^{(2)}[\mathbf{r}; \mathbf{p}, -\mathbf{p}] \right. \\ \left. + \int_{\mathbf{q}} \Gamma_{k,33j}^{(3)}[\mathbf{r}; \mathbf{p}, -\mathbf{p}, \mathbf{q}] \partial_t r_j(\mathbf{q}) \right] \Big|_{\mathbf{r}=\mathbf{r}_{0,k}}. \end{aligned} \quad (52)$$

Using the flow equation Eq. (30), the flow of ζ_k obtained from Eq. (35), as well as the explicit expression of the three-point vertex

$$\begin{aligned} \Gamma_{k,iij}^{(3)}[\mathbf{r}; \mathbf{p}, -\mathbf{p}, \mathbf{q}] \Big|_{\mathbf{r}_{0,k}} = -i \zeta_k \left[2\mu_k \theta(2-i) q_i \mathbf{p}^2 \delta_{ij} \right. \\ \left. + 2\theta(2-i)(\lambda_k + \mu_k) \delta_{ij} (\mathbf{p} \cdot \mathbf{q}) p_i \right. \\ \left. + \theta(2-j)(2\mu_k p_j \mathbf{p} \cdot \mathbf{q} + \lambda_k \mathbf{p}^2 q_j) \right], \end{aligned} \quad (53)$$

(with no summation over the index i), one obtains the RG flow equations for the running couplings λ_k , μ_k , ζ_k and for the field renormalization Z_k .

As usual, it is convenient to introduce dimensionless couplings constants \bar{g}_k . They are given by:

$$\zeta_k = k^{\eta_k} \bar{\zeta}_k, \quad \lambda_k = k^{2-2\eta_k} \bar{\lambda}_k, \quad \mu_k = k^{2-2\eta_k} \bar{\mu}_k \quad (54)$$

where η_k is the (scale-dependent) anomalous dimension such that:

$$Z_k = k^{-\eta_k}. \quad (55)$$

One thus obtain [40]:

$$\begin{aligned} \partial_t \bar{\lambda}_k = & (-2 + 2\eta_k) \bar{\lambda}_k \\ & + \frac{A_2}{\bar{\zeta}_k^2(\bar{\lambda}_k + \bar{\mu}_k)} \left[\bar{\lambda}_k^2 \bar{\mu}_k \bar{\zeta}_k^2 (25\bar{L}_{002}^6 + 10\bar{L}_{020}^6 + 6\bar{L}_{200}^6) \right. \\ & + \bar{\lambda}_k^3 \bar{\zeta}_k^2 (7\bar{L}_{002}^6 + 2\bar{L}_{020}^6 + 2\bar{L}_{200}^6) \\ & + \bar{\mu}_k^3 \bar{\zeta}_k^2 (9\bar{L}_{002}^6 + 8\bar{L}_{020}^6 + \bar{L}_{200}^6) \\ & + 4\bar{\mu}_k^2 (\bar{L}_{001}^4 - \bar{L}_{010}^4) + 2\bar{\lambda}_k \bar{\mu}_k (\bar{L}_{001}^4 - \bar{L}_{010}^4) \\ & \left. + \bar{\lambda}_k \bar{\mu}_k^2 \bar{\zeta}_k^2 (27\bar{L}_{002}^6 + 16\bar{L}_{020}^6 + 5\bar{L}_{200}^6) \right] \\ \partial_t \bar{\mu}_k = & (-2 + 2\eta_k) \bar{\mu}_k \\ & + \frac{A_2}{\bar{\zeta}_k^2(\bar{\lambda}_k + \bar{\mu}_k)} \left[2\bar{\mu}_k (\bar{\lambda}_k + 2\bar{\mu}_k) (\bar{L}_{010}^4 - \bar{L}_{001}^4) \right. \\ & + \bar{\zeta}_k^2 (\bar{\lambda}_k + \bar{\mu}_k) (3\bar{\mu}_k + \bar{\lambda}_k)^2 \bar{L}_{002}^6 \\ & \left. + \bar{\zeta}_k^2 \bar{\mu}_k^2 (\bar{\lambda}_k + \bar{\mu}_k) \bar{L}_{200}^6 \right] \\ \partial_t \bar{\zeta}_k^2 = & -\eta_k \bar{\zeta}_k^2 \\ & + \frac{2A_2}{\bar{\mu}_k + \bar{\lambda}_k} \left[\bar{\lambda}_k (2\bar{L}_{001}^4 + \bar{L}_{010}^4 + \bar{L}_{100}^4) \right. \\ & \left. + \bar{\mu}_k (3\bar{L}_{001}^4 + 2\bar{L}_{010}^4 + \bar{L}_{100}^4) \right] \end{aligned} \quad (56)$$

while the expression of $\eta_k = -\partial_t \ln Z_k$ which is too long to be given here, is provided in Appendix A. In Eq. (56) one has $A_2 = 1/8\pi$.

In Eqs. (56), we have introduced the so-called threshold functions [57, 58, 60, 61], which encode the contribution of fluctuations at scale k . In the context of membranes they are defined as [40]

$$L_{abc}^{2+\alpha} = -\frac{1}{4A_2} \hat{\partial}_t \int_{\mathbf{q}} \mathbf{q}^\alpha G_{k,0}(\mathbf{q})^a G_{k,1}(\mathbf{q})^b G_{k,2}(\mathbf{q})^c, \quad (57)$$

where the propagators are given by

$$G_{k,i}(\mathbf{q})^{-1} = P(\mathbf{q}) + m_{i,k}^2 \mathbf{q}^2, \quad P(\mathbf{q}) = Z_k \mathbf{q}^4 + R_k(\mathbf{q}), \quad (58)$$

with

$$m_{0,k}^2 = 0, \quad m_{1,k}^2 = \zeta_k^2 \mu_k, \quad m_{2,k}^2 = \zeta_k^2 (\lambda_k + 2\mu_k). \quad (59)$$

The dimensionless counterparts of the threshold functions, $\bar{L}_{abc}^{2+\alpha}$, which are the ones entering Eqs. (56), are related to the $L_{abc}^{2+\alpha}$ by

$$L_{abc}^{2+\alpha} = (Z_k k^4)^{-a-b-c} k^{2+\alpha} \bar{L}_{abc}^{2+\alpha}. \quad (60)$$

Their explicit expressions in terms of dimensionless quantities are given in App. B 1.

4. RG equations in the flat phase

The renormalization group equations relevant for the flat phase are obtained from the generic flow equations Eq. (56) by taking the limit in which the phonon modes decouple from the theory. This corresponds to the regime where the running scale k becomes small compared to the phonon pseudo-masses,

denoted generically by $m_{p,k}$. These dimensionful pseudo-masses behave as

$$m_{p,k}^2 \propto k^2 \bar{\zeta}_k^2 \bar{g}_k, \quad (61)$$

where \bar{g}_k stands for either $\bar{\mu}_k$ or $\bar{\lambda}_k + 2\bar{\mu}_k$, and $\bar{\zeta}_k$ is the dimensionless stretching factor. In practice, the phonon decoupling is thus realized on condition that

$$\bar{\zeta}_k^2 \bar{g}_k \gg 1. \quad (62)$$

Since the \bar{g}_k 's approach finite values at the flat-phase fixed point, this condition is equivalent to taking a very large dimensionless stretching factor,

$$\bar{\zeta}_k \gg 1. \quad (63)$$

In this limit one recovers the flat-phase RG equations [40]:

$$\begin{cases} \partial_t \bar{\lambda}_k = 2(\eta_k - 1) \bar{\lambda}_k + (2\bar{\lambda}_k^2 + 4\bar{\lambda}_k \bar{\mu}_k + \bar{\mu}_k^2) A_2 \bar{L}_{200}^6 \\ \partial_t \bar{\mu}_k = 2(\eta_k - 1) \bar{\mu}_k + \bar{\mu}_k^2 A_2 \bar{L}_{200}^6 \end{cases} \quad (64)$$

The only threshold that survives is a “massless” one \bar{L}_{200}^6 . As for the running anomalous dimension η_k in the flat phase it is given by [40]:

$$\begin{aligned} \eta_k = 2A_2(\bar{\lambda}_k + 2\bar{\mu}_k) \bar{N}_{200}^4 \\ - \frac{2A_2}{(\bar{\lambda}_k + 2\bar{\mu}_k)} (\bar{\lambda}_k^2 + \bar{\lambda}_k \bar{\mu}_k + \bar{\mu}_k^2) \bar{L}_{100}^2 \end{aligned} \quad (65)$$

with the massless threshold functions given by [40]:

$$\begin{cases} L_{a00}^{2+\alpha} = -\frac{1}{4A_2} \hat{\partial}_t \int_q \mathbf{q}^\alpha P(\mathbf{q})^{-a} \\ N_{a00}^{2+\alpha} = -\frac{1}{4A_2} \hat{\partial}_t \int_q \mathbf{q}^\alpha \frac{\partial P(\mathbf{q})}{\partial \mathbf{q}^2} P(\mathbf{q})^{-a} \end{cases} \quad (66)$$

The dimensionless threshold functions $\bar{N}_{a00}^{2+\alpha}$ that enter in Eq. (65) are related to the dimensionful threshold function by:

$$N_{abc}^{2+\alpha} = (Z_k k^4)^{-a-b-c} Z_k k^{4+\alpha} \bar{N}_{abc}^{2+\alpha}. \quad (67)$$

Their expressions in terms of dimensionless quantities are given in Appendix B 1.

Considering the Litim cut-off, see the Appendix B 1 c, the RG equations of the coupling constants and the running anomalous dimension read [40]:

$$\begin{cases} \partial_t \bar{\lambda}_k = 2(\eta_k - 1) \bar{\lambda}_k + \frac{(2\bar{\lambda}_k^2 + 4\bar{\lambda}_k \bar{\mu}_k + \bar{\mu}_k^2)(10 - \eta_k)}{60\pi} \\ \partial_t \bar{\mu}_k = 2(\eta_k - 1) \bar{\mu}_k + \frac{\bar{\mu}_k^2(10 - \eta_k)}{60\pi} \\ \eta_k = \frac{6\bar{\mu}_k(\bar{\lambda}_k + \bar{\mu}_k)}{\bar{\mu}_k(\bar{\lambda}_k + \bar{\mu}_k) + 4\pi(\bar{\lambda}_k + 2\bar{\mu}_k)} \end{cases} \quad (68)$$

One can also introduce the Young modulus $Y_k = 4\mu_k(\lambda_k + \mu_k)/(\lambda_k + 2\mu_k)$. In terms of this variable the flow reads :

$$\begin{cases} \partial_t \bar{Y}_k = 2(\eta_k - 1) \bar{Y}_k + \frac{(10 - \eta_k)}{80\pi} \bar{Y}_k^2 \\ \eta_k = \frac{6\bar{Y}_k}{16\pi + \bar{Y}_k} \end{cases} \quad (69)$$

The expressions Eqs. (68) and (69) are remarkably simple. Nevertheless, they provide an excellent description of the flat phase of membrane monolayers. In particular, at the infrared fixed point characterizing the flat phase, one finds [40]

$$\bar{\mu}_* \simeq 6.21, \quad \bar{\lambda}_* \simeq -3.10, \quad Y_* \simeq 8.29, \quad (70)$$

and, finally, an anomalous exponent [40]

$$\eta \simeq 0.849, \quad (71)$$

which is the value obtained both within the present approximation and in computations including wavevector-dependent elastic couplings [41, 42].

5. Cutoff dependence

Note finally that, in this article, we use a specific cutoff function – namely the Litim cutoff – which yields extremely simple analytical expressions for the RG equations (68) or (69). In principle, one should vary this choice and even consider whole families of cut-off functions, labeled by one or several parameters and optimized accordingly, see, e.g., Refs. [65, 71, 72]. Indeed, once the effective average action is truncated, a residual dependence on the regulator is indeed unavoidable, and optimizing the cut-off function then allows one to minimize this dependence. However, the results obtained for the flat phase of membranes are known to be very robust with respect to the choice of cut-off, see Ref. [40]. Moreover, the extreme stability of the results upon enriching the ansatz – either by including higher powers of the order parameter [40] or by allowing the coupling constants to acquire a wavevector dependence $g_k(\mathbf{q})$ [42] – provides additional support for this robustness.

C. Bilayers

Now, let us investigate the case of membrane bilayers. The running Gibbs free energy, expressed in terms of fields \mathbf{r} and \mathbf{s} reads [45]:

$$\begin{aligned} \Gamma_k[\mathbf{r}, \mathbf{s}] = & \int d^2x \left\{ \frac{Z_k}{2} \left(2(\partial^2 \mathbf{r})^2 + \frac{1}{2}(\partial^2 \mathbf{s})^2 \right) + \lambda_k u_{\alpha\alpha}^2 \right. \\ & + 2\mu_k u_{\alpha\beta}^2 + \frac{\lambda_k}{4} (\partial_\alpha \mathbf{r} \cdot \partial_\alpha \mathbf{s})^2 + \frac{\mu_k}{4} (\partial_\alpha \mathbf{s} \cdot \partial_\beta \mathbf{r})^2 \\ & + \frac{\lambda_k}{64} (\partial_\alpha \mathbf{s} \cdot \partial_\alpha \mathbf{s})^2 + \frac{\mu_k}{32} (\partial_\alpha \mathbf{s} \cdot \partial_\beta \mathbf{s})^2 + \frac{\lambda_k}{4} u_{\alpha\alpha} \partial_\beta \mathbf{s} \cdot \partial_\beta \mathbf{s} \\ & + \frac{\mu_k}{2} u_{\alpha\beta} \partial_\alpha \mathbf{s} \cdot \partial_\beta \mathbf{s} + \frac{\mu_k}{4} (\partial_\alpha \mathbf{r} \cdot \partial_\beta \mathbf{s})(\partial_\alpha \mathbf{s} \cdot \partial_\beta \mathbf{r}) \\ & \left. + \frac{g_{1k}}{8\ell_k^4} (\mathbf{s}^2 - \ell_k^2)^2 + \frac{g_{2k}}{2\ell_k^2} (\mathbf{s} \cdot \partial_\alpha \mathbf{r})^2 + \frac{g_{3k}}{4\ell_k^2} (\mathbf{s}^2 - \ell_k^2) u_{\alpha\alpha} \right\}. \end{aligned} \quad (72)$$

Starting from this expression, we will perform a few simplifications. First, we will consider the case of an infinite coupling g_{1k} , so that the constraint $|\mathbf{S}|^2 = \ell_k^2$ is effectively enforced. It then follows automatically that the volume-area term $(\mathbf{S}^2 - \ell_k^2) u_{\alpha\alpha}$,

proportional to g_{3k} , does not contribute, so that one puts $g_{3k} \equiv 0$. Next, in the flat phase, we consider both a low-wavevector limit, $\mathbf{q}^2 \ell^2 \ll \zeta^2$ and a regime where g_{2k} is very large which simplifies the spectrum of excitations. Owing to the fact that these two limits do not commute, this procedure leads to a very specific form of the flexural propagator and, ultimately, to the mechanical rigidity crossover, see below.

Another approximation concerns the RG treatment of the bilayer action Eq. (72). In the naive construction of $\Gamma_k[\mathbf{r}, \mathbf{s}]$, no distinction is made between different monomials: for instance, the same field renormalization factor Z_k appears in front of both $(\partial^2 \mathbf{r})^2$ and $(\partial^2 \mathbf{s})^2$, and the same coupling constants λ_k and μ_k are used for different invariants built from \mathbf{r} and \mathbf{s} . This is not the most general situation; in principle, one should assign distinct couplings, indexed by the specific monomial to which they belong. For the sake of simplicity, however, we shall restrict ourselves in this work to the simplified parametrization described

above.

1. Derivation of the RG flow: general

The derivation of the RG flow proceeds exactly as in the monolayer case, except that the bilayer action Eq. (72) now involves the additional couplings $g_{1,k}$ and $g_{2,k}$, which couple the two layers.

2. Propagators

We now give the expression of the propagator in the flat phase defined by Eq. (9) that writes in a RG context as :

$$\begin{cases} \mathbf{r}_{0,k} = \zeta_k x_\alpha \mathbf{e}_\alpha, \\ \mathbf{s}_{0,k} = \ell_k \mathbf{n} . \end{cases} \quad (73)$$

One first needs the second functional derivative $\Gamma_k^{(2)}[\mathbf{r}, \mathbf{s}; \mathbf{q}, -\mathbf{q}]$ evaluated in this configuration, hereafter denoted by the subscript FP :

$$\Gamma_k^{(2)}[\mathbf{r}, \mathbf{s}; \mathbf{q}, -\mathbf{q}]|_{FP} = \begin{pmatrix} \Gamma_{k,rr}[\mathbf{r}, \mathbf{s}; \mathbf{q}, -\mathbf{q}] & \mathbf{0}_{2 \times 3} & \mathbf{0}_{2 \times 1} \\ \mathbf{0}_{3 \times 2} & \Gamma_{k,rs}[\mathbf{r}, \mathbf{s}; \mathbf{q}, -\mathbf{q}] & \mathbf{0}_{3 \times 1} \\ \mathbf{0}_{1 \times 2} & \mathbf{0}_{1 \times 3} & \Gamma_{k,ss}[\mathbf{r}, \mathbf{s}; \mathbf{q}, -\mathbf{q}] \end{pmatrix} \Big|_{FP} . \quad (74)$$

Here, $\Gamma_{k,rr}$ describes the pure center-of-mass sector, $\Gamma_{k,ss}$ the pure relative-displacement sector, and $\Gamma_{k,rs}$

(together with its transpose $\Gamma_{k,sr}$) encodes the mixing between the \mathbf{r} and \mathbf{s} sectors.

One has:

$$\Gamma_{k,rr}^{(2)}[\mathbf{r}, \mathbf{s}; \mathbf{q}, -\mathbf{q}]|_{FP} = \begin{pmatrix} 2Z_k \mathbf{q}^4 + 2M_1[\mathbf{q}^2] & 2\zeta_k^2(\lambda_k + \mu_k)q_1 q_2 \\ 2\zeta_k^2(\lambda_k + \mu_k)q_1 q_2 & 2Z_k \mathbf{q}^4 + 2M_2[\mathbf{q}^2] \end{pmatrix} \quad (75)$$

$$\Gamma_{k,rs}^{(2)}[\mathbf{r}, \mathbf{s}; \mathbf{q}, -\mathbf{q}]|_{FP} = \begin{pmatrix} 2Z_k \mathbf{q}^4 + q_1^2 g_{2k} & -\frac{ig_{2k}\zeta_k q_1}{\ell_k} & \frac{ig_{2k}\zeta_k q_1}{\ell_k} \\ \frac{ig_{2k}\zeta_k q_1}{\ell_k} & \frac{1}{2}Z_k \mathbf{q}^4 + \frac{1}{2}\zeta_k^2 \frac{2g_{2k}}{\ell_k^2} + \frac{1}{2}M_1[\mathbf{q}^2] & \frac{1}{2}\zeta_k^2(\lambda_k + \mu_k)q_1 q_2 \\ \frac{ig_{2k}\zeta_k q_2}{\ell_k} & \frac{1}{2}\zeta_k^2(\lambda_k + \mu_k)q_1 q_2 & \frac{1}{2}Z_k \mathbf{q}^4 + \frac{1}{2}\zeta_k^2 \frac{2g_{2k}}{\ell_k^2} + \frac{1}{2}M_2[\mathbf{q}^2] \end{pmatrix} \quad (76)$$

with $M_i[\mathbf{q}^2] = \zeta_k^2(\mu_k \mathbf{q}^2 + (\lambda_k + \mu_k)q_i^2)$ and

$$\Gamma_{k,ss}^{(2)}[\mathbf{r}, \mathbf{s}; \mathbf{q}, -\mathbf{q}]|_{FP} = \frac{Z_k}{2} \mathbf{q}^4 + \frac{g_{1k}}{\ell_k^2} . \quad (77)$$

The eigenvalues of $[\Gamma_{k,ij}^{(2)}|_{FP} + R_k(\mathbf{q})]^{-1}$ can be easily extracted.

• In the rr -sector one gets:

$$\begin{cases} G_{k,1rr}(\mathbf{q}) = \frac{1}{2(Z_k \mathbf{q}^4 + m_{1,k}^2 \mathbf{q}^2 + R_k(\mathbf{q}))} \\ G_{k,2rr}(\mathbf{q}) = \frac{1}{2(Z_k \mathbf{q}^4 + m_{2,k}^2 \mathbf{q}^2 + R_k(\mathbf{q}))} . \end{cases} \quad (78)$$

The propagators $G_{k,1rr}(\mathbf{q})$ and $G_{k,2rr}(\mathbf{q})$ are associated with the phonon modes of the mean membrane and are characterized by squared pseudo-masses $m_{1,k}^2 = \zeta_k^2 \mu_k$ and $m_{2,k}^2 = \zeta_k^2 (\lambda_k + 2\mu_k)$, respectively, which are identical to those of a membrane monolayer. Up to overall factors of 1/2, these propagators coin-

cide with the monolayer expressions given in Eqs. (46) and (47).

- In the ss -sector one has:

$$G_{k,ss}(\mathbf{q}) = \frac{2}{Z_k \mathbf{q}^4 + 2m_{ss,k}^2 + R_k(\mathbf{q})}. \quad (79)$$

The propagator $G_{k,ss}(\mathbf{q})$ is associated with the flexural mode of the relative membrane. It is characterized by a genuine squared mass

$$m_{ss,k}^2 = \frac{g_{1,k}}{\ell_k^2}, \quad (80)$$

which reflects the breaking of translational invariance along the direction orthogonal to the membranes. In the following, we shall focus on the regime where the coupling $g_{1,k}$ is much larger than the other couplings. We therefore take the limit $g_{1,k} \rightarrow \infty$, in which $G_{k,ss}(\mathbf{q})$ vanishes and the interlayer distance remains fixed.

- In the rs sector, one obtains a first propagator

$$G_{k,1rs}(\mathbf{q}) = \frac{2}{Z_k \mathbf{q}^4 + m_{1,k}^2 \mathbf{q}^2 + m_{rs,k}^2 + R_k(\mathbf{q})}, \quad (81)$$

with

$$m_{rs,k}^2 = \frac{2\zeta_k^2 g_{2,k}}{\ell_k}. \quad (82)$$

Because of the presence of the coupling $g_{2,k}$, the explicit expressions of the two remaining propagators in this sector are rather lengthy and are therefore relegated to App. C.

Since we are interested in long-distance physics, we may consider the low-wavevector limit, $\mathbf{q}^2 \ell^2 \ll \zeta^2$ together with that of large- g_2 coupling constant. In this regime, a second propagator takes the form

$$G_{k,2rs}(\mathbf{q}) = \frac{2}{Z_k \mathbf{q}^4 + m_{2,k}^2 \mathbf{q}^2 + m_{rs,k}^2 + R_k(\mathbf{q})}. \quad (83)$$

The propagators $G_{k,1rs}$ and $G_{k,2rs}$ are associated with phonon modes of the relative membrane and exhibit two distinct kinds of masses: the squared pseudo-masses $m_{1,k}^2$ and $m_{2,k}^2$ as well as the genuine squared masses $m_{rs,k}^2$ arising from the coupling between the membranes. Again the propagators $G_{k,1rs}$ and $G_{k,2rs}$ deduce from those of monolayers by a factor 2.

The second, and most important, propagator obtained in the low-wavevector, large- g_2 limits reads

$$G_{k,3rs}(\mathbf{q}) = \frac{1}{2((Z_k + c_k) \mathbf{q}^4 + R_k(\mathbf{q}))}, \quad (84)$$

with

$$c_k = \ell_k^2 \frac{\lambda_k + 2\mu_k}{4}. \quad (85)$$

The propagator $G_{k,3rs}(\mathbf{q})$ is associated with the flexural mode of the mean membrane and carries neither a mass nor a pseudo-mass. As can be seen from

Eq. (84), its explicit dependence on $g_{2,k}$ has disappeared (see App. C). However, because the limits $\mathbf{q} \rightarrow 0$ and $g_{2,k} \rightarrow 0$ do not commute, the signature of a finite interlayer coupling $g_{2,k}$ remains encoded in the specific form of $G_{k,3rs}$.

Indeed, Eqs. (84) and (85) show that the bending rigidity is shifted with respect to the monolayer case, compare Eq. (48), according to

$$\kappa \longrightarrow \kappa_{\text{eff}} = \kappa + c_k. \quad (86)$$

This is precisely the modification obtained by de Andrés *et al.* [52] within a harmonic treatment. It constitutes the main effect of adding the interlayer coupling $g_{2,k}$ to the monolayer membrane theory and is responsible for the crossover of the running coupling constants along the RG flow.

3. Physical discussion: origin of the combination $\ell^2(\lambda + 2\mu)/2$

We now discuss the origin of the combination $\ell^2(\lambda + 2\mu)/2$ that appears in the effective bending rigidity κ_{eff} . This contribution originates from the interlayer shear coupling, which converts in-plane compression and shear of the two coupled layers into an additional bending energy for the mean membrane. We now show this in more detail.

We first recall the physical situation. The interlayer distance is strictly fixed by the large- g_1 constraint $\mathbf{s}^2 \simeq \ell^2$. The term proportional to g_2 also plays a crucial geometric role. Writing the relative field as

$$\mathbf{s} = s_n \mathbf{n} + \mathbf{s}_{\parallel}, \quad (87)$$

with \mathbf{n} the local normal to the mean surface and \mathbf{s}_{\parallel} its tangential component, one has, for small slopes, $\mathbf{s} \cdot \partial_{\alpha} \mathbf{r} \simeq \mathbf{s}_{\parallel} \cdot \partial_{\alpha} \mathbf{r}$. The contribution

$$\frac{g_2}{2\ell^2} (\mathbf{s} \cdot \partial_{\alpha} \mathbf{r})^2 \quad (88)$$

therefore penalizes precisely the tangential component \mathbf{s}_{\parallel} , i.e. lateral sliding between the two layers at fixed normal separation. In the regime where g_2 is large, the relative field is thus effectively constrained to be normal to the mean surface, $\mathbf{s} \simeq \ell \mathbf{n}$, so that the bilayer behaves as two parallel membranes, separated by a fixed distance ℓ , without in-plane slip.

We now consider a purely bending deformation of the bilayer and make this explicit by working in the Monge representation. We parameterize the mean surface as

$$\mathbf{r}(x, y) = (x, y, h(x, y)), \quad (89)$$

and, for simplicity, we first restrict to a uniaxial bending mode with $h = h(x)$ and small slopes, $|\partial_x h| \ll 1$. In this setting, the mean surface acts as a neutral surface for bending, while the two physical layers 1 and 2, parametrized by the vectors

$$\mathbf{r}_1 = \mathbf{r} + \frac{\ell}{2} \mathbf{n}, \quad \mathbf{r}_2 = \mathbf{r} - \frac{\ell}{2} \mathbf{n} \quad (90)$$

experience opposite in-plane strains along the bending direction.

To make this more precise, we use the expression of the metric $g_{\alpha\beta}(d)$ induced at a distance d from a reference surface with metric $g_{\alpha\beta}$. One has, see App. D

$$g_{\alpha\beta}(d) = g_{\alpha\beta} - 2d K_{\alpha\beta} + d^2 (K^2)_{\alpha\beta}, \quad (91)$$

where $K_{\alpha\beta}$ is the second fundamental form and $(K^2)_{\alpha\beta}$ the corresponding quadratic curvature tensor.

In our case one has $d = +\ell/2$ and $d = -\ell/2$. Plugging these values into Eq. (91) and expanding to first order in ℓ , we obtain

$$g_{\alpha\beta}^{(1,2)} = g_{\alpha\beta} \mp \ell K_{\alpha\beta} + O(\ell^2), \quad (92)$$

where the sign corresponds to the choice $\pm\ell/2$ along the normal \mathbf{n} and where the indices and 2 refer to the corresponding surfaces.

The strain tensor on each surface is defined (with our conventions) as

$$u_{\alpha\beta}^{(i)} = \frac{1}{2} (g_{\alpha\beta}^{(i)} - \delta_{\alpha\beta}), \quad i = 1, 2. \quad (93)$$

Let $g_{\alpha\beta}^{(0)} := g_{\alpha\beta}$ and

$$u_{\alpha\beta}^{(0)} = \frac{1}{2} (g_{\alpha\beta}^{(0)} - \delta_{\alpha\beta}) \quad (94)$$

be the strain of the mean surface. Using Eq. (92), we can write

$$u_{\alpha\beta}^{(1,2)} = u_{\alpha\beta}^{(0)} \mp \frac{\ell}{2} K_{\alpha\beta} + O(\ell^2). \quad (95)$$

For a pure bending mode of the mean surface (neutral surface), we can neglect $u_{\alpha\beta}^{(0)}$ and keep only the curvature-induced part:

$$u_{\alpha\beta}^{(1)} \simeq -\frac{\ell}{2} K_{\alpha\beta}, \quad u_{\alpha\beta}^{(2)} \simeq +\frac{\ell}{2} K_{\alpha\beta}. \quad (96)$$

The in-plane elastic energy density of a single layer with Lamé coefficients λ, μ is

$$f_{\text{el}} = \lambda u_{\alpha\alpha}^2 + 2\mu u_{\alpha\beta}^2. \quad (97)$$

For the uniaxial bending mode described above (say $h = h(x)$ in Monge gauge), one principal curvature direction dominates, and we can effectively take

$$u_{xx}^{(1,2)} \simeq \pm \frac{\ell}{2} \kappa, \quad u_{yy}^{(1,2)} \simeq u_{xy}^{(1,2)} \simeq 0, \quad (98)$$

where $\kappa \sim \partial_x^2 h$ is the local curvature.

In this uniaxial case,

$$u_{\alpha\alpha} = u_{xx} = \varepsilon, \quad u_{\alpha\beta}^2 = u_{xx}^2 = \varepsilon^2, \quad (99)$$

so the elastic energy for each sheet is

$$f_{\text{el}}^{(i)} = (\lambda + 2\mu) (\varepsilon^{(i)})^2. \quad (100)$$

Substituting $\varepsilon^{(1,2)} = \pm(\ell/2) \kappa$, we obtain

$$f_{\text{el}}^{(1)} = (\lambda + 2\mu) \left(\frac{\ell}{2} \kappa \right)^2, \quad f_{\text{el}}^{(2)} = (\lambda + 2\mu) \left(-\frac{\ell}{2} \kappa \right)^2, \quad (101)$$

and the total elastic energy density associated with bending of the bilayer is

$$\begin{aligned} f_{\text{el}}^{(\text{bilayer})} &= f_{\text{el}}^{(1)} + f_{\text{el}}^{(2)} \\ &= 2(\lambda + 2\mu) \frac{\ell^2}{4} \kappa^2 \\ &= \frac{\ell^2}{2} (\lambda + 2\mu) \kappa^2. \end{aligned} \quad (102)$$

In Monge gauge, $\kappa \sim \partial_x^2 h$, so this is a contribution of the form

$$\frac{\ell^2}{2} (\lambda + 2\mu) (\partial^2 h)^2 \quad (103)$$

in the effective average action for the mean surface. It is thus natural to interpret

$$\kappa_{\text{el}} = \frac{\ell^2}{2} (\lambda + 2\mu) \quad (104)$$

as the elastic bending rigidity induced by the in-plane elasticity of the two layers, once the bilayer geometry $\mathbf{r} \pm \ell \mathbf{n}/2$ is enforced by the large- g_1 , large- g_2 limit.

4. RG equations in the flat phase

We now derive the RG equation, considering straight away the flat phase limit.

The definitions of the coupling constants does not change – up to factors 1/2 – with respect the monolayer case and are given by:

$$\begin{cases} \mu_k = \frac{1}{2\zeta_k^2} \lim_{\mathbf{p} \rightarrow 0} \frac{\partial}{\partial \mathbf{p}^2} (\Gamma_{k,22}^{(2)}[\mathbf{r}, \mathbf{s}; \mathbf{p}, -\mathbf{p}]) \Big|_{FP} \\ \lambda_k = \frac{1}{2\zeta_k^2} \lim_{\mathbf{p} \rightarrow 0} \frac{\partial}{\partial \mathbf{p}_2^2} (\Gamma_{k,22}^{(2)}[\mathbf{r}, \mathbf{s}; \mathbf{p}, -\mathbf{p}]) \Big|_{FP} - \mu_k \\ Z_k = \frac{1}{2} \lim_{\mathbf{p} \rightarrow 0} \frac{\partial}{\partial \mathbf{p}^4} (\Gamma_{k,33}^{(2)}[\mathbf{r}, \mathbf{s}; \mathbf{p}, -\mathbf{p}]) \Big|_{FP} \end{cases} \quad (105)$$

while ζ_k is defined in the same way as in Eq.(34).

We proceed in the same way as in the monolayer case and introduce dimensionless couplings. We define

$$\begin{aligned} \lambda_k &= k^{2-2\eta_k} \bar{\lambda}_k, & \mu_k &= k^{2-2\eta_k} \bar{\mu}_k, \\ \zeta_k &= k^{\eta_k} \bar{\zeta}_k & \ell_k &= k^{(-2+\eta_k)/2} \bar{\ell}_k \end{aligned} \quad (106)$$

and the running anomalous dimension as

$$Z_k = k^{-\eta_k}. \quad (107)$$

We are only interested in the flat phase of the system. We can therefore take, prior to the calculation, the limit $\bar{\zeta}_k \gg 1$. The RG equations that control the infrared behaviour of membrane bilayers are then given by:

$$\begin{cases} \partial_t \bar{\lambda}_k = 2(\eta_k - 1) \bar{\lambda}_k + (2\bar{\lambda}_k^2 + 4\bar{\lambda}_k \bar{\mu}_k + \bar{\mu}_k^2) A_2 B \bar{L}_{200}^6 \\ \partial_t \bar{\mu}_k = 2(\eta_k - 1) \bar{\mu}_k + \frac{1}{2} \bar{\mu}_k^2 A_2 B \bar{L}_{200}^6 \\ \eta_k = (\bar{\lambda}_k + 2\bar{\mu}_k) A_2 B \bar{N}_{200}^4 \\ \quad - \frac{(\bar{\lambda}_k^2 + \bar{\lambda}_k \bar{\mu}_k + \bar{\mu}_k^2) A_2 B \bar{L}_{100}^2}{\bar{\lambda}_k + 2\bar{\mu}_k} \end{cases} \quad (108)$$

Once again, these equations are remarkably simple. In fact, they differ from those of monolayer membranes, Eqs. (64) and (65), only by the rescalings

$$\lambda_k \rightarrow \frac{\lambda_k}{2}, \quad \mu_k \rightarrow \frac{\mu_k}{2}, \quad (109)$$

and by the replacement of the threshold functions

$$\bar{T}_{a00}^{2+\alpha} \rightarrow {}_B\bar{T}_{a00}^{2+\alpha}, \quad T = L, N. \quad (110)$$

The new, bilayer-specific threshold functions are defined as, see App. B 2

$$\begin{cases} {}_B L_{a00}^{2+\alpha} = -\frac{1}{4A_2} \hat{\partial}_t \int_{\mathbf{q}} \mathbf{q}^\alpha P_{c_k}(\mathbf{q})^{-a}, \\ {}_B N_{a00}^{2+\alpha} = -\frac{1}{4A_2} \hat{\partial}_t \int_{\mathbf{q}} \mathbf{q}^\alpha \frac{\partial P_{c_k}(\mathbf{q})}{\partial \mathbf{q}^2} P_{c_k}(\mathbf{q})^{-a}, \end{cases} \quad (111)$$

where the only difference between the monolayer and bilayer cases lies in the definition of $P_{c_k}(\mathbf{q})$, which now reads

$$P_{c_k}(\mathbf{q}) = (Z_k + c_k) \mathbf{q}^4 + R_k(\mathbf{q}). \quad (112)$$

Using the Litim cut-off (see App. B 2c), the RG flow equations for the coupling constants in the flat phase take the form:

$$\begin{cases} \partial_t \bar{\lambda}_k = 2(\eta_k - 1) \bar{\lambda}_k - H_k (2\bar{\lambda}_k^2 + 4\bar{\lambda}_k \bar{\mu}_k + \bar{\mu}_k^2), \\ \partial_t \bar{\mu}_k = 2(\eta_k - 1) \bar{\mu}_k - H_k \bar{\mu}_k^2 \end{cases} \quad (113)$$

with:

$$H_k \equiv \frac{1}{128\pi \bar{c}_k^{5/2} (1 + \bar{c}_k)^2} \left[\sqrt{\bar{c}_k} \left((1 + \bar{c}_k)(3 + \bar{c}_k) \eta_k - 4(\bar{c}_k - 1) \bar{c}_k \right) + (1 + \bar{c}_k)^2 \left(\bar{c}_k(\eta_k - 4) - 3\eta_k \right) \times \text{ArcTan}[\sqrt{\bar{c}_k}] \right]. \quad (114)$$

For the Young modulus, one has:

$$\partial_t \bar{Y}_k = 2(\eta_k - 1) \bar{Y}_k - \frac{3}{4} H_k \bar{Y}_k^2, \quad (115)$$

while η_k , expressed in terms of \bar{Y}_k , is given by:

$$\eta_k = \frac{12 \bar{Y}_k \bar{c}_k \left(\sqrt{\bar{c}_k} + (1 + \bar{c}_k) \text{ArcTan}[\sqrt{\bar{c}_k}] \right)}{(1 + \bar{c}_k) \left[3 \bar{Y}_k (\bar{c}_k - 1) \text{ArcTan}[\sqrt{\bar{c}_k}] + \sqrt{\bar{c}_k} (3 \bar{Y}_k + 128\pi \bar{c}_k) \right]}. \quad (116)$$

In Eqs. (114) and (116) one has

$$\bar{c}_k = \bar{\ell}_k^2 \frac{\bar{\lambda}_k + 2\bar{\mu}_k}{4}, \quad (117)$$

which induces a nontrivial dependence of the flow on $\bar{\ell}_k$, $\bar{\lambda}_k$ and $\bar{\mu}_k$. We finally give the flow equation for the parameter $\bar{\ell}_k$, which characterizes the rest distance between the two membranes. Since the physical separation ℓ is fixed, the flow of $\bar{\ell}_k$ is purely dimensional and is simply given by

$$\partial_t \bar{\ell}_k = \frac{2 - \eta_k}{2} \bar{\ell}_k \quad (118)$$

and that of \bar{c}_k by:

$$\partial_t \bar{c}_k = \eta_k \bar{c}_k - H_k \bar{c}_k \frac{2\bar{\lambda}_k^2 + 4\bar{\lambda}_k \bar{\mu}_k + 3\bar{\mu}_k^2}{\bar{\lambda}_k + 2\bar{\mu}_k}. \quad (119)$$

It is easy to check that in the limit $\bar{\ell}_k \rightarrow 0$, thus $\bar{c}_k \rightarrow 0$, the equations Eqs. (115) and (116) give those of monolayers Eq. (69).

IV. PHYSICAL RESULTS

We now turn to a discussion of our results. We begin in Sec. IV A with a qualitative analysis of the short- and long-distance behaviour of the effective bending rigidity, from which we obtain an estimate of the mechanical crossover scale k_c . In Sec. IV B, we

specify the initial conditions of the RG flow for realistic (graphene) parameter values. We then discuss, in Sec. IV C, the Ginzburg scale k_G associated with the harmonic-anharmonic crossover. Finally, in Sec. IV D, we study the flow of the running anomalous dimension and Young modulus.

A. Mechanical crossover scale

Here we analyze the short- and long-distance behaviour of the effective bending rigidity and provide an estimate of the mechanical crossover length scale.

As recalled above, the effective bending rigidity of the mean surface contains two contributions:

$$\kappa_{\text{eff}}(k) \simeq \underbrace{2\kappa_k}_{\text{microscopic bending}} + \underbrace{\frac{\ell^2}{2}(\lambda_k + 2\mu_k)}_{\text{elastic bilayer contribution}}. \quad (120)$$

It is worth stressing at this point that our NPRG approach naturally provides a scale-dependent effective bending rigidity $\kappa_{\text{eff}}(k)$, while most experimental determinations of κ extract an effective value averaged over a finite wave-vector window set by the sample geometry and the probing technique (nanoindentation, snap-through, modal analysis, or scattering). In this sense, measurements typically probe $\kappa_{\text{eff}}(k \simeq k_{\text{geom}})$, with $k_{\text{geom}} \sim 1/L$ the inverse size of the probed membrane or the typical wave vector of the relevant mode,

rather than the strict $k \rightarrow 0$ limit. The RG description in terms of $\kappa_{\text{eff}}(k)$ is therefore particularly well suited to interpret these experiments, since it directly encodes how the apparent bending rigidity changes when the probed length scale is varied.

For bilayers, the crossover between the “thick-plate” regime and the two-monolayer regime predicted by our RG flow should manifest itself as a strong dependence of the effective bending rigidity on the probed length scale, in qualitative agreement with the thickness- and size-dependent stiffness reported in recent experiments and simulations on few-layer graphene.

1. Short- and long-distance behaviour of the effective bending rigidity

In the RG framework, it is convenient to work with dimensionless couplings $\bar{\lambda}_k, \bar{\mu}_k, \bar{\kappa}_k$ defined as :

$$\lambda_k = k^{2-2\eta_k} \bar{\lambda}_k, \quad \mu_k = k^{2-2\eta_k} \bar{\mu}_k, \quad \kappa_k = k^{-\eta_k} \bar{\kappa}_k, \quad (121)$$

with $\{\bar{\lambda}_k, \bar{\mu}_k, \bar{\kappa}_k, \eta_k\} \rightarrow \{\bar{\lambda}_*, \bar{\mu}_*, \bar{\kappa}_*, \eta\}$ as $k \rightarrow 0$. The physical interlayer distance, ℓ is kept fixed, so that we do not make ℓ dimensionless. Using the scaling forms (121), the two pieces of $\kappa_{\text{eff}}(k)$ in Eq.(120) read

$$\begin{cases} \kappa_{\text{mi}}(k) \equiv 2\kappa_k = 2\bar{\kappa}_k k^{-\eta_k}, \\ \kappa_{\text{el}}(k) \equiv \frac{\ell^2}{2}(\lambda_k + 2\mu_k) = \frac{\ell^2}{2}(\bar{\lambda}_k + 2\bar{\mu}_k) k^{2-2\eta_k}. \end{cases} \quad (122)$$

a. Short-distance regime. At high RG scales k , the geometric elastic contribution associated with the finite interlayer distance ℓ is already present, while the microscopic bending rigidity has not yet undergone its full anomalous growth. If the bare combination $\ell^2(\bar{\lambda}_k + 2\bar{\mu}_k)/2$ is sufficiently large at the microscopic scale, the UV effective bending rigidity is dominated by the elastic contribution,

$$\kappa_{\text{eff}}(k) \simeq \kappa_{\text{el}}(k) = \frac{\ell^2}{2}(\bar{\lambda}_k + 2\bar{\mu}_k) k^{2-2\eta_k}. \quad (123)$$

b. Long-distance regime. At long distance the dimensionless coupling constants $\bar{\lambda}_k, \bar{\mu}_k$ and $\bar{\kappa}_k$ approach the flat-phase fixed point, so the k -dependence is fully contained in the powers of k :

$$\kappa_{\text{mi}}(k) \propto k^{-\eta}, \quad \kappa_{\text{el}}(k) \propto \ell^2 k^{2-2\eta}. \quad (124)$$

In $D = 2$ one has $0 < \eta < 1$, so

$$-\eta < 0, \quad 2 - 2\eta > 0. \quad (125)$$

Therefore, as $k \rightarrow 0$,

$$\kappa_{\text{mi}}(k) \rightarrow \infty, \quad \kappa_{\text{el}}(k) \rightarrow 0, \quad (126)$$

and the effective bending rigidity is dominated by the renormalized microscopic bending term,

$$\kappa_{\text{eff}}(k) \simeq 2\kappa_k \propto k^{-\eta}. \quad (127)$$

2. Mechanical crossover scale : first analysis

The crossover scale k_c between these two regimes is determined by the condition

$$\frac{\ell^2}{2}(\lambda_{k_c} + 2\mu_{k_c}) \simeq 2\kappa_{k_c}, \quad (128)$$

which expresses the competition, along the RG flow, between the elastic bending stiffness generated by the in-plane couplings $\bar{\lambda}_k, \bar{\mu}_k$ at fixed physical separation ℓ and the anomalously growing microscopic bending rigidity κ_k .

Note that, in terms of purely dimensionless coupling, this is equivalent to:

$$\frac{\ell_k^2}{2}(\bar{\lambda}_{k_c} + 2\bar{\mu}_{k_c}) \simeq 2\bar{\kappa}_{k_c} \quad (129)$$

which gives :

$$\bar{\kappa}_{k_c} \simeq 1. \quad (130)$$

If k_c lies in the scaling regime of the flat phase, the dimensionless couplings are already close to their fixed-point values:

$$\bar{\lambda}_{k_c} \simeq \bar{\lambda}_*, \quad \bar{\mu}_{k_c} \simeq \bar{\mu}_*, \quad \bar{\kappa}_{k_c} \simeq \bar{\kappa}_*, \quad \eta_{k_c} \simeq \eta. \quad (131)$$

Under this approximation, Eq. (129) gives the simple estimate

$$\ell^2(\bar{\lambda}_* + 2\bar{\mu}_*) k_c^{2-\eta} \simeq 4\bar{\kappa}_*, \quad (132)$$

so that

$$k_c \sim \left[\frac{4\bar{\kappa}_*}{\ell^2(\bar{\lambda}_* + 2\bar{\mu}_*)} \right]^{\frac{1}{2-\eta}}. \quad (133)$$

Numerically, with the bare values of graphene [45] $\kappa_* = \kappa_g = 1$, and $\ell = \ell_g = 3.25 \text{ \AA}$ and the fixed point values [40]: $\bar{\mu}_* \simeq 6.21, \bar{\lambda}_* \simeq -3.10, \eta = 0.85$ and [40] one gets: $k_c \simeq 0.06 \text{ \AA}^{-1}$ and the RG-time $t_c = -\ln k_c a = 1.88$.

Alternatively one could use the bare coupling constants

$$k_c \sim a^{-1} \left[\frac{4\bar{\kappa}}{\ell^2(\bar{\lambda} + 2\bar{\mu})} \right]^{\frac{1}{2-\eta}}. \quad (134)$$

If one considers those of the graphene [45]:

$$\begin{aligned} \kappa_g &= 1 \text{ eV} & \lambda_g &= 3.8 \text{ eV \AA}^{-2} & \mu_g &= 9.3 \text{ eV \AA}^{-2} \\ \ell_g &= 3.25 \text{ \AA} & a_g &= 2.46 \text{ \AA} \end{aligned} \quad (135)$$

one gets: $k_c \simeq 0.012 \text{ \AA}^{-1}$ and the RG-time $t_c = -\ln k_c a = 3.54$.

An improved estimate of k_c is provided below.

3. Mechanical crossover scale : comparison with prior work

It is interesting to consider the mechanical crossover scales obtained in presence of an explicit g_2 -dependence as considered by Mauri *et al.* [45]. One

has [45]:

$$\begin{cases} k_{1c} = \sqrt{\frac{g_2}{2\kappa}}, \\ k_{2c} = \frac{1}{\ell} \sqrt{\frac{2g_2}{\lambda + 2\mu}}. \end{cases} \quad (136)$$

For the representative value $g_2 = 0.11$ used in Ref. [45], these expressions yield the orders of magnitude

$$k_{1c} \simeq 0.23 \text{ \AA}^{-1}, \quad k_{2c} \simeq 0.03 \text{ \AA}^{-1}, \quad (137)$$

and the corresponding RG ‘‘times’’

$$t_{1c} = -\ln(k_{1c}a) \simeq 0.55, \quad t_{2c} = -\ln(k_{2c}a) \simeq 2.60. \quad (138)$$

However, within the present approach these scales are only indicative, since (i) the coupling g_2 drops out at leading order, and (ii) we work with renormalized rather than bare quantities. Nevertheless it is interesting to note that the bare quantity $\bar{c}_{k=a^{-1}}$ is nothing but the squared ratio $(k_{1c}/k_{2c})^2$. Thus:

- When $\bar{c}_{k=a^{-1}}$ is large, i.e. $k_{1c} \gg k_{2c}$, the effective rigidity is dominated by the elastic contribution,

$$\kappa_{\text{eff}} \simeq \frac{\ell^2}{2} (\lambda + 2\mu). \quad (139)$$

- When $\bar{c}_{k=a^{-1}}$ is of order unity, i.e. $k_{1c} \sim k_{2c}$, the bending rigidity κ and the elastic couplings λ and μ contribute on an equal footing, and

$$\kappa_{\text{eff}} \simeq 2\kappa + \frac{\ell^2}{2} (\lambda + 2\mu). \quad (140)$$

- When $\bar{c}_{k=a^{-1}}$ is small, i.e. $k_{1c} \ll k_{2c}$, in-plane elasticity becomes negligible for bending and the two monolayers bend together; one then recovers a regime dominated by the bending rigidity of two independent monolayers,

$$\kappa_{\text{eff}} \simeq 2\kappa. \quad (141)$$

We therefore have a natural correspondence between the parameter c_k and the problem’s natural crossover scales.

4. Mechanical crossover scale : RG analysis

We finally provide an estimate of the mechanical crossover scale k_c based on an RG analysis. We define the crossover RG-time t_c as the scale at which $\bar{c}_{k_c} \simeq 1$, see Eq.(130). For a temperature $T = 500$ K, one finds $k_c \simeq 0.0028 \text{ \AA}^{-1}$ and $t_c \simeq 4.96$, see Fig. 3, which is larger than both t_{1c} and t_{2c} .

As seen in Fig. 3, the typical crossover RG-time t_c lies well above the two scales t_{1c} and t_{2c} , see Eq.(138), between which the rigidity crossover would naively be expected to occur. The origin of this discrepancy is the following. When g_2 is kept finite, the mechanical

crossover observed in Ref. [45] is driven by interlayer shear, characterized by g_2 , and naturally takes place between t_{1c} and t_{2c} . In the present case, where we consider the limit of large g_2 , we define the crossover scale by

$$\frac{\ell^2}{2} (\lambda_{k_c} + 2\mu_{k_c}) \simeq 2\kappa_{k_c}, \quad (142)$$

which marks the scale at which the microscopic (running) bending contribution $2\kappa_k$ and the (running) elastic thick-plate contribution $\ell^2(\lambda_k + 2\mu_k)/2$ to the effective bending rigidity become equal. In the flat phase, κ_k increases under the RG flow whereas λ_k and μ_k decrease, so that this balance is reached only deep in the infrared. As a consequence, the crossover RG-time $t_c = \ln(k_c/k_0)$ is much larger than the bare mechanical crossover times t_{1c} and t_{2c} defined at the harmonic level in terms of the bare coupling constants. It therefore reflects a fully renormalized internal bending/elastic balance rather than a bare sliding crossover.

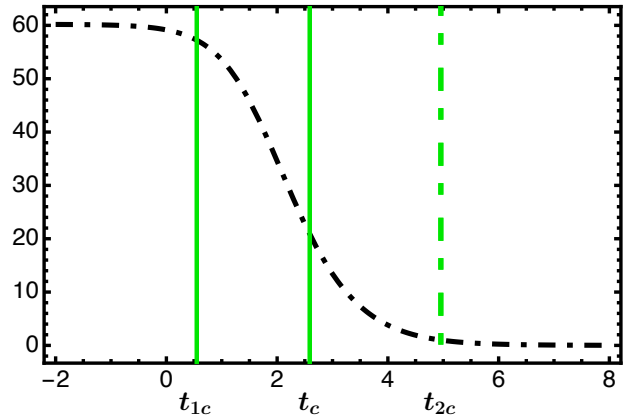


FIG. 3. Behaviour of \bar{c}_k – dashed-dot curve – as a function of $t = -\ln ka$ for $T = 500$ K. One has displayed the typical RG-time t_c (dashed-dot vertical line) associated with the bending rigidity crossover and the RG-times t_{1c} and t_{2c} (full vertical lines).

The different wavevector scales given above should be compared with the wave-vector windows (or, equivalently, length scales) effectively probed in experiments and simulations, rather than with absolute values of the bending rigidity. In particular, the crossover between the elasticity-dominated and curvature-dominated regimes encoded in $\kappa_{\text{eff}}(k)$ provides a natural framework to rationalize the strong thickness dependence observed in bilayer and few-layer graphene [46, 50, 51] as well as the size- and temperature-dependent effective rigidities inferred from modal analysis and helium-atom scattering [47, 48].

B. Initial conditions RG flow: graphene parameters

We give here the initial conditions of the flow. We restore the physical units of the coupling constants

and consider the microscopic scale $k = a^{-1}$:

$$\begin{aligned}\bar{\lambda}_{k=a^{-1}} &= k^{-2+2\eta_k} Z_k^2 \beta^{-1} \kappa^{-2} \lambda_g|_{k=a^{-1}} = \frac{k_B T a^2}{\kappa^2} \lambda_g \\ \bar{\mu}_{k=a^{-1}} &= k^{-2+2\eta_k} Z_k^2 \beta^{-1} \kappa^{-2} \mu_g|_{k=a^{-1}} = \frac{k_B T a^2}{\kappa^2} \mu_g \\ \bar{\ell}_{k=a^{-1}} &= k^{(4-D+\eta_k)/2} \sqrt{\frac{\beta \kappa}{Z_k}} \ell_g|_{k=a^{-1}} = \sqrt{\frac{\kappa}{k_B T}} \frac{\ell_g}{a}\end{aligned}\quad (143)$$

If we again use the physical coupling constants of graphene, we obtain

$$\bar{c}_{k=a^{-1}} = \frac{\ell_g^2}{4\kappa} (\lambda_g + 2\mu_g) \simeq 59.15, \quad (144)$$

which is much larger than unity. We are therefore precisely in the conditions required to observe a mechanical crossover.

C. Ginzburg scale

One finally define the Ginzburg scale which sets the harmonic-to-anharmonic crossover. For a monolayer, is given by [17, 28]

$$k_{G,\text{mono}} = \sqrt{\frac{3TY}{16\pi\kappa^2}}. \quad (145)$$

For bilayers, Mauri *et al.* [45] have defined:

$$\begin{cases} k_{1G} = \sqrt{\frac{3T}{16\pi} \frac{(2Y)}{(2\kappa)^2}} \\ k_{2G} = \sqrt{\frac{3T}{16\pi} \frac{(2Y)}{(\kappa_0)^2}} \end{cases} \quad (146)$$

where $Y = 4\mu(\lambda + \mu)/(\lambda + 2\mu)$ is the Young modulus and $\kappa_0 = 2\kappa + \ell^2 \frac{\lambda + 2\mu}{2}$.

We introduce the corresponding RG-times

$$t_{1G} = -\ln(k_{1G}a), \quad t_{2G} = -\ln(k_{2G}a). \quad (147)$$

These scales are associated with the thermal crossover between the harmonic regime, for $t \ll t_{1G}, t_{2G}$, and the anharmonic (renormalized) regime, for $t \gg t_{1G}, t_{2G}$.

Numerically, for $T = 500$ K, one finds

$$k_{1G} \simeq 0.16 \text{ A}^{-1}, \quad k_{2G} \simeq 0.027 \text{ A}^{-1}, \quad (148)$$

corresponding to

$$t_{1G} \simeq 0.89, \quad t_{2G} \simeq 4.98. \quad (149)$$

A harmonic-to-anharmonic RG-time scale that is more directly relevant to the present RG study is given, for instance, by the scale at which the anomalous dimension, obtained from the RG equation Eqs. (113), (115) and (116), becomes of order its fixed-point value η . More precisely, we impose

$$\eta_{k_G} = \omega \eta, \quad (150)$$

with ω a number of order unity (e.g. $\omega = 1/2$), so that for $k \gg k_G$ the flow remains close to the harmonic (Gaussian) regime with $\eta_k \simeq 0$, while for $k \ll k_G$ it is governed by the nontrivial flat-phase fixed point with $\eta_k \simeq \eta$.

At a temperature $T = 500$ K one finds $k_G = 1.82$, as defined in Eq.(150), and $t_G = 1.50$, that lies between t_{1G} and t_{2G} as defined in Eq.(146), see Fig.(4). This turns out to be true at all temperatures. From now on, we will consider t_G as the harmonic-to-anharmonic crossover RG-time scale.

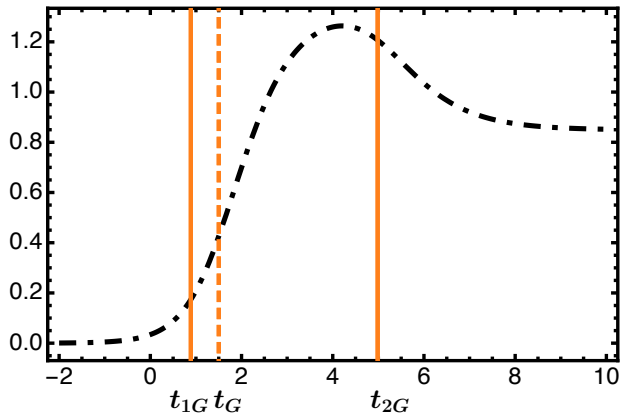


FIG. 4. Behaviour of η_k – dashed curve – as a function of $t = -\ln ka$ for $T = 500$ K; One gives also the typical Ginzburg RG-time scale t_G (dashed vertical line) and the bare Ginzburg RG-time scales t_{G1} and t_{G2} (full vertical lines).

D. RG analysis

We now present our results, which concern the RG evolution of both the running anomalous dimension η_k , given by Eq. (116) and the running Young modulus $\bar{Y}_k = 4\bar{\mu}_k(\bar{\lambda}_k + \bar{\mu}_k)/(\bar{\lambda}_k + 2\bar{\mu}_k)$, given by Eq. (115), for various temperatures. We have considered $T = 10$ K, $T = 100$ K and $T = 1000$ K. In each case, we indicate the Ginzburg scale t_G by a vertical dotted line and the mechanical crossover scale t_c by a vertical dot-dashed line.

As in Ref. [45], it is instructive to compare the flows for bilayers with those for monolayers, in order to disentangle the rigidity crossover specific to bilayers from the harmonic-to-anharmonic crossover that occurs in both systems.

As a preliminary remark, we find that the harmonic-anharmonic crossover scale t_G and the mechanical crossover scale t_c shift with temperature in a strongly correlated way, so that their separation along the RG flow remains essentially constant. This is naturally understood within the RG picture: both t_G and t_c are defined by fixed conditions on functions of the same running dimensionless couplings (e.g. η_k and the ratio $\ell^2(\lambda_k + 2\mu_k)/(4\kappa_k)$), along a unique renormalized trajectory in coupling space. Changing the microscopic parameters (such as T) mainly shifts the entry point on this trajectory, which translates all characteristic

scales in the RG-time t by approximately the same amount. As a result, the difference $\Delta t = t_G - t_c$, and hence the relative position of the two crossovers, is nearly temperature independent.

1. Behaviour of the anomalous dimension η_k^B

In Fig.(5), (6) and (7) we have represented the anomalous dimensions of a bilayer η_k^B and that of a monolayer η_k^m at the temperatures $T = 10\text{K}$, $T = 100\text{K}$ and $T = 1000\text{K}$. First, one observes that at large times, the RG flow of the anomalous dimension of a bilayer converges towards that of a monolayer that, itself, reaches the value taken at the IR fixed point of the flat phase: $\eta \simeq 0.85$. Second, one sees that harmonic-to-anharmonic crossover takes place long before the mechanical one, and that, at all temperatures. Third, one observes that the two crossovers occur at earlier and earlier RG-times when the temperature increases, as expected.

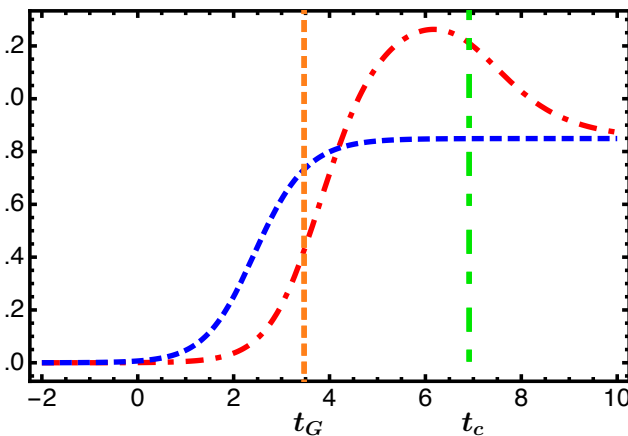


FIG. 5. The flow of the anomalous dimension at $T = 10\text{K}$. Dashed-dot curve : η_k^B of a bilayer; dashed curve : η_k^m of a monolayer; dotted vertical lines : the Ginzburg RG-time t_G ; dashed-dot vertical line : the mechanical crossover RG-time t_c .

Then, comparing the behaviour of η_k^B and η_k^m one also observes that the former stays longer in the harmonic regime ($\eta_k = 0$) than the latter one. This relies on the very structure of η_k^B which is such that, at the beginning of the flow, *i.e.* at large \bar{c}_k , one has

$$\eta_k^B \underset{\bar{c}_k \gg 1}{=} \frac{3}{64} \frac{\bar{Y}_K}{\sqrt{\bar{c}_k}} + \mathcal{O}\left(\frac{1}{\bar{c}_k}\right) \quad (151)$$

and is thus small. This effect is obviously all the more pronounced at low temperature as fluctuations are small. Then one observes that η_k^B varies in a relatively moderate way with \bar{c}_k with only a slight peak – of order 50% with respect to the monolayer case – in the region bounded by the harmonic-to-anharmonic crossover and the mechanical crossover. Expanding η_k^B at small \bar{c}_k one gets:

$$\eta_k^B \underset{\bar{c}_k \ll 1}{=} \frac{6\bar{Y}_K}{\bar{Y}_K + 32\pi} + \mathcal{O}(\bar{c}_k) . \quad (152)$$

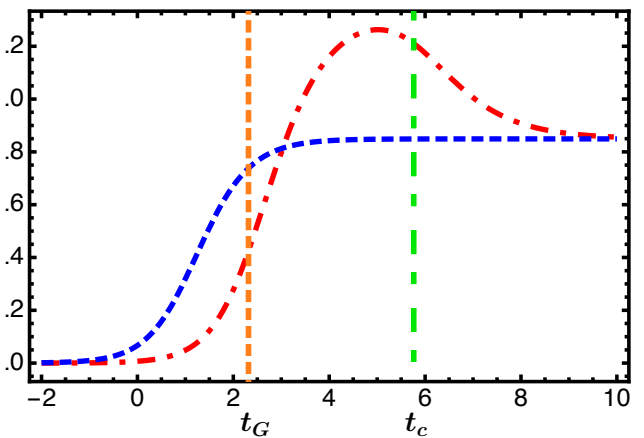


FIG. 6. The flow of the anomalous dimension at $T = 100\text{K}$. Dashed-dot curve : η_k^B of a bilayer; dashed curve : η_k^m of a monolayer; dotted vertical lines : the Ginzburg RG-time t_G ; dashed-dot vertical line : the mechanical crossover RG-time t_c .

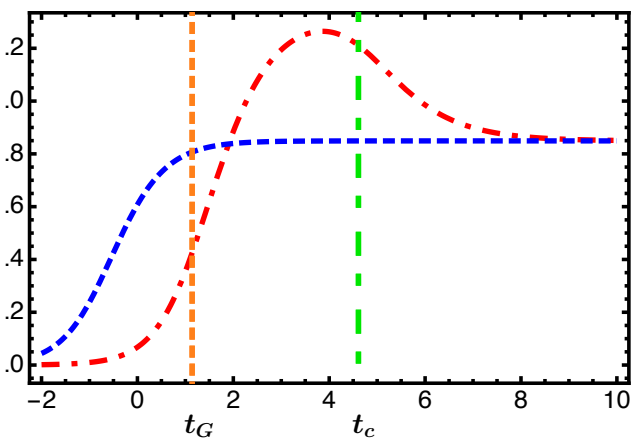


FIG. 7. The flow of the anomalous dimension at $T = 1000\text{K}$. Dashed-dot curve : η_k^B of a bilayer; dashed curve : η_k^m of a monolayer; dotted vertical lines : the Ginzburg RG-time t_G ; dashed-dot vertical line : the mechanical crossover RG-time t_c .

The dependence on \bar{c}_k is therefore smooth and only appears at linear order in \bar{c}_k near $\bar{c}_k = 0$: when going from \bar{c}_k to a moderately nonzero \bar{c}_k , η_k^B changes only moderately.

2. Behaviour of the Young modulus \bar{Y}_K^B

In Figs. 8, 9 and 10, we show the running Young modulus \bar{Y}_K^B of a bilayer together with the quantity $2\bar{Y}_k^m$ corresponding to two uncoupled monolayers, for temperatures $T = 10\text{K}$, $T = 100\text{K}$ and $T = 1000\text{K}$. Once again, we observe that at large RG-times the flow of the bilayer Young modulus \bar{Y}_K^B converges towards $2\bar{Y}_k^m$, which itself approaches the value at the infrared fixed point of the flat phase, characterized by $\bar{\mu}_*^m \simeq 6.21$, $\bar{\lambda}_*^m \simeq -3.10$, and hence $2\bar{Y}_*^m \simeq 16.57$.

As for the anomalous dimension, the harmonic-to-anharmonic crossover takes place well before the mechanical crossover, and both crossover scales are

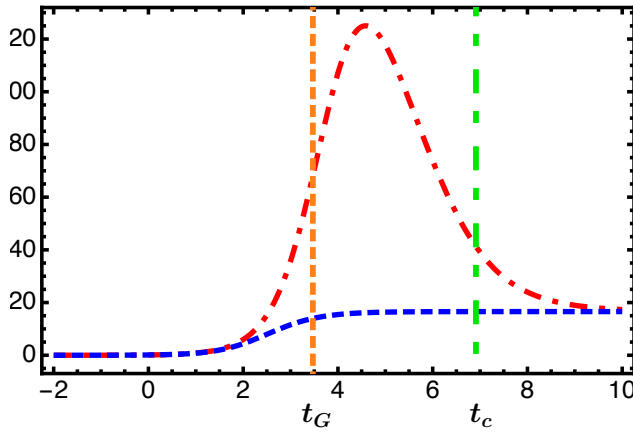


FIG. 8. The flow of the Young modulus at $T = 10\text{K}$. Dashed-dot curve : \bar{Y}_K^B of a bilayer; dashed curve : \bar{Y}_K^m of a monolayer; dotted vertical lines : the Ginzburg RG-time t_G ; dashed-dot vertical line : the mechanical crossover RG-time t_c .

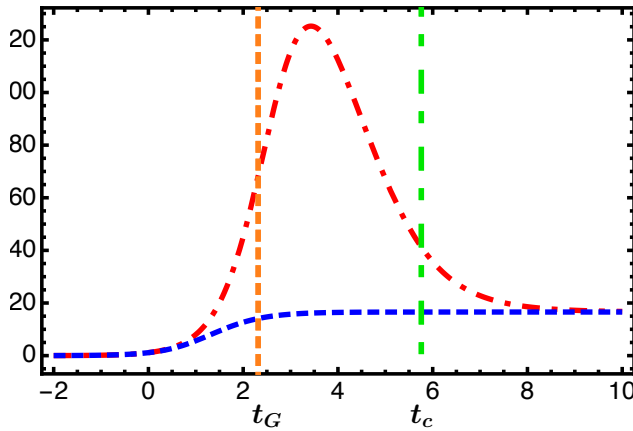


FIG. 9. The flow of the Young modulus at $T = 100\text{K}$. Dashed-dot curve : \bar{Y}_K^B of a bilayer; dashed curve : \bar{Y}_K^m of a monolayer; dotted vertical lines : the Ginzburg RG-time t_G ; dashed-dot vertical line : the mechanical crossover RG-time t_c .

shifted to earlier RG-times as the temperature T is increased.

In this case, we see that \bar{Y}_k^B exhibits a behaviour that differs drastically from that of a monolayer: it displays a very pronounced peak of order 650% with respect to the monolayer value in the window between the harmonic-to-anharmonic crossover and the mechanical crossover. This phenomenon is again straightforward to analyze. To do so, let us consider the RG flow equation for \bar{Y}_k^B

$$\partial_t \bar{Y}_k = 2(\eta_k - 1) \bar{Y}_k - \frac{3}{4} H_k \bar{Y}_k^2, \quad (153)$$

and examine how the interplay between the running couplings λ_k , μ_k and the scale dependence of $\kappa_{\text{eff},k}$ amplifies the transient growth of the bilayer Young modulus before it eventually relaxes towards its fixed-point value.

In Eq. (153) the dependence with respect to \bar{c}_k appears both in η_k and H_k . For large \bar{c}_k , η_k is, as seen

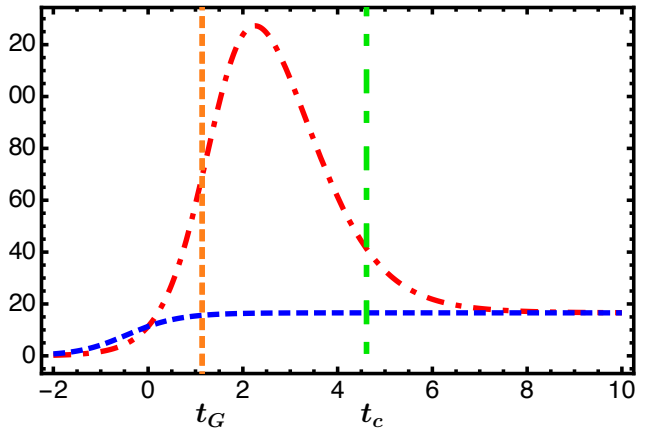


FIG. 10. The flow of the Young modulus at $T = 1000\text{K}$. Dashed-dot curve : \bar{Y}_K^B of a bilayer; dashed curve : \bar{Y}_K^m of a monolayer; dotted vertical lines : the Ginzburg RG-time t_G ; dashed-dot vertical line : the mechanical crossover RG-time t_c .

above, only slightly modified. However the behaviour of H_k is given by

$$H_k \underset{\bar{c}_k \gg 1}{=} -\frac{1}{64 \bar{c}_k^{3/2}} + \mathcal{O}\left(\frac{1}{\bar{c}_k^2}\right). \quad (154)$$

Thus, for an initial value of \bar{c}_k relatively large, H_k is very small so that the nonlinear term in the flow of \bar{Y}_K , Eq. (153), is strongly suppressed at the beginning of the flow which is quasi-linear:

$$\partial_t \bar{Y}_k \simeq 2(\eta_k - 1) \bar{Y}_k. \quad (155)$$

On the other hand for $\bar{c}_k \ll 1$, H_k behaves as:

$$H_k \underset{\bar{c}_k \ll 1}{=} -\frac{\bar{Y}_k + 80\pi}{30\pi(\bar{Y}_k + 32\pi)} + \mathcal{O}(\bar{c}_k) \quad (156)$$

and is thus of order unity, the nonlinear term in Eq. (153) becomes important as soon as \bar{Y}_K becomes large. From these two behaviours one can thus expect a rapid change (a jump) of \bar{Y}_K in a transient phase.

V. CONCLUSION

In this work, we have studied elastic bilayers within a nonperturbative renormalization group framework, starting from the simplest possible action written in terms of the mean field \mathbf{R} and the relative field \mathbf{S} . We have shown that this description reproduces in a controlled way the crossover of the effective bending rigidity previously identified within a self-consistent approach: at short distances the rigidity is dominated by the combination $\ell^2(\lambda + 2\mu)/2$, while at large distances it tends to 2κ . The key difference is that, within the RG formalism, the elastic nonlinearities neglected in the self-consistent treatment are now explicitly included, providing a more coherent picture of the crossover regime. More fundamentally, the formalism used here, unlike the self-consistent method, in no way requires nonlinearities to be neglected at the structural level. On the contrary, it is possible to consider

an action as general as possible and to treat all the associated fluctuations. We also recall the rotationally invariant form of the action used, which stands in clear contrast to those employed in the perturbative framework.

To return to the explicit results, from a formal point of view, the flow equations obtained for the bilayer have exactly the same structure as those of a single polymerized membrane but with a propagator for the flexuron field modified by an additional term. This shows that, in our formalism, going from a monolayer to a bilayer does not require any new conceptual machinery: it simply amounts to applying the same flow equations to an enlarged set of fields and combinations of fields.

These remarks naturally open several directions for future work:

(i) As a first step, one can relax the assumption of a common field renormalization for both fields \mathbf{R} and \mathbf{S} and, more generally, of identical couplings for different kinds of monomials allowed by symmetry and entering in the action. In particular, it would make it possible to follow separately the renormalization of the symmetric and antisymmetric sectors and to test the robustness of the crossover scenario when the two modes acquire different anomalous dimensions. In the same spirit, the action can be enriched by terms involving higher powers of the fields \mathbf{R} and \mathbf{S} . Although simple power-counting and RG relevance arguments suggest that such contributions should remain subdominant for large-scale elasticity, including them explicitly would provide an *a posteriori* check of this expectation and a test of the stability of the critical exponents and crossover lengths.

(ii) Another natural extension is to treat wavevector-dependent couplings, that is, to work with a genuinely \mathbf{q} -dependent ansatz for the effective Lamé coefficients and bending rigidities of the \mathbf{R} and \mathbf{S} modes. This would give a more refined description of the crossover region between the regimes dominated by projected elasticity and by the renormalized bending rigidity.

(iii) One can then include explicitly the dependence on g_2 and, more generally, on various interlayer couplings like g_1 and g_3 in the flow equations. This would allow a more quantitative characterization of how interlayer couplings feeds into the effective infrared bending rigidity of the bilayer.

(iv) The present formalism can also be generalized to asymmetric bilayers, with different elastic and curvature properties for each sheet. Allowing for different bare rigidities and Lamé coefficients on the two

layers would bring the model closer to realistic systems where the two membranes are not mechanically identical. Finally, one can introduce spontaneous curvatures (possibly distinct for each layer or for specific modes) and investigate their impact on the flow of couplings and on the phase structure, in particular on the locking of the relative mode and on the average geometry of the bilayer.

From a phenomenological perspective, it is natural to view the short-scale regime $\kappa_{\text{eff}} \simeq \ell^2(\lambda + 2\mu)/2$ and the long-scale regime $\kappa_{\text{eff}} \simeq 2\kappa$ as the continuum counterparts of the distinct behaviours reported in recent experiments and simulations on few-layer graphene. The large apparent bending rigidity measured for bilayers in buckling and snap-through experiments [46] the pronounced softening and change of scaling under strong bending in trilayers and thicker stacks due to interlayer slip [50] and the observed size- and temperature-dependent effective stiffness in suspended membranes all point to a complex crossover structure [47, 48, 51]. In addition, atomistic Monte Carlo and molecular-dynamics simulations of bilayer and few-layer graphene also reveal a thickness-dependent flexural response and a crossover from correlated to uncorrelated layer fluctuations, further highlighting the role of interlayer coupling in the long-wavelength mechanical behaviour [28, 49]. Within our NPRG framework, this complexity is encoded in the flow of $\kappa_{\text{eff}}(k)$ and the associated crossover scale k_c , which can be directly compared to the wave-vector windows effectively probed in these measurements and numerical studies.

The present work provides a first coherent nonperturbative RG framework for elastic bilayers, simple enough to remain tractable, yet already rich enough to support a broad range of systematic extensions able to tackle a wide variety of experimental and numerical situations.

ACKNOWLEDGMENTS

L.D. and D.M. greatly thank A. Mauri for illuminating discussions.

Appendix A: Running anomalous dimension

We give here the expression of the running anomalous dimensions in the monolayer case in D dimensions. One has:

$$\begin{aligned}
\eta_k = & \frac{A_D}{\bar{\zeta}_k^4 \bar{\mu}_k (\bar{\lambda}_k + 2\bar{\mu}_k)} \left(-2\bar{\zeta}_k^4 \bar{\mu}_k (\bar{\lambda}_k^2 + \bar{\lambda}_k \bar{\mu}_k + \bar{\mu}_k^2) \bar{L}_{100}^D + \bar{\zeta}_k^8 \bar{\lambda}_k \bar{\mu}_k^4 \bar{L}_{030}^{D+4} + 2\bar{\zeta}_k^8 \bar{\mu}_k^5 \bar{L}_{030}^{D+4} + \bar{\zeta}_k^6 \bar{\mu}_k^3 (\bar{\lambda}_k + 2\bar{\mu}_k) \bar{L}_{020}^{D+2} \right. \\
& + 3\bar{\zeta}_k^8 \bar{\lambda}_k^4 \bar{\mu}_k \bar{L}_{003}^{D+4} + 24\bar{\zeta}_k^8 \bar{\lambda}_k^3 \bar{\mu}_k^2 \bar{L}_{003}^{D+4} + 72\bar{\zeta}_k^8 \bar{\lambda}_k^2 \bar{\mu}_k^3 \bar{L}_{003}^{D+4} + 96\bar{\zeta}_k^8 \bar{\lambda}_k \bar{\mu}_k^4 \bar{L}_{003}^{D+4} + 48\bar{\zeta}_k^8 \bar{\mu}_k^5 \bar{L}_{003}^{D+4} - \bar{\zeta}_k^6 \bar{\lambda}_k^3 \bar{\mu}_k \bar{L}_{002}^{D+2} \\
& - 8\bar{\zeta}_k^6 \bar{\lambda}_k^2 \bar{\mu}_k^2 \bar{L}_{002}^{D+2} - 20\bar{\zeta}_k^6 \bar{\lambda}_k \bar{\mu}_k^3 \bar{L}_{002}^{D+2} - 16\bar{\zeta}_k^6 \bar{\mu}_k^4 \bar{L}_{002}^{D+2} + 2\bar{\zeta}_k^4 \bar{\mu}_k (\bar{\lambda}_k^2 + \bar{\lambda}_k \bar{\mu}_k + \bar{\mu}_k^2) \bar{L}_{001}^D + \bar{\zeta}_k^2 \bar{\lambda}_k \bar{\mu}_k \bar{M}_{020}^{D+2} \\
& + 2\bar{\zeta}_k^2 \bar{\mu}_k^2 \bar{M}_{020}^{D+2} + 2\bar{\lambda}_k \bar{M}_{010}^D + 4\bar{\mu}_k \bar{M}_{010}^D + \bar{\zeta}_k^6 \bar{\lambda}_k \bar{\mu}_k^3 \bar{N}_{030}^{D+4} + 2\bar{\zeta}_k^6 \bar{\mu}_k^4 \bar{N}_{030}^{D+4} + 3\bar{\zeta}_k^4 \bar{\lambda}_k \bar{\mu}_k^2 \bar{N}_{020}^{D+2} + 6\bar{\zeta}_k^4 \bar{\mu}_k^3 \bar{N}_{020}^{D+2} \\
& + 5\bar{\zeta}_k^2 \bar{\lambda}_k \bar{\mu}_k \bar{N}_{010}^D + 10\bar{\zeta}_k^2 \bar{\mu}_k^2 \bar{N}_{010}^D + 3\bar{\zeta}_k^2 \bar{\lambda}_k \bar{\mu}_k \bar{M}_{002}^{D+2} + 6\bar{\zeta}_k^2 \bar{\mu}_k^2 \bar{M}_{002}^{D+2} + 6\bar{\mu}_k \bar{M}_{001}^D + 3\bar{\zeta}_k^6 \bar{\mu}_k (\bar{\lambda}_k + 2\bar{\mu}_k)^3 \bar{N}_{003}^{D+4} \\
& + 5\bar{\zeta}_k^4 \bar{\lambda}_k^2 \bar{\mu}_k \bar{N}_{002}^{D+2} + 18\bar{\zeta}_k^4 \bar{\lambda}_k \bar{\mu}_k^2 \bar{N}_{002}^{D+2} + 16\bar{\zeta}_k^4 \bar{\mu}_k^3 \bar{N}_{002}^{D+2} + 7\bar{\zeta}_k^2 \bar{\lambda}_k \bar{\mu}_k \bar{N}_{001}^D + 10\bar{\zeta}_k^2 \bar{\mu}_k^2 \bar{N}_{001}^D + 4\bar{\zeta}_k^2 \bar{\lambda}_k \bar{\mu}_k \bar{M}_{200}^{D+2} \\
& + 8\bar{\zeta}_k^2 \bar{\mu}_k^2 \bar{M}_{200}^{D+2} - 2\bar{\lambda}_k \bar{M}_{100}^D - 10\bar{\mu}_k \bar{M}_{100}^D + 2\bar{\zeta}_k^4 \bar{\lambda}_k \bar{\mu}_k \bar{N}_{200}^{D+2} + 8\bar{\zeta}_k^4 \bar{\lambda}_k \bar{\mu}_k^2 \bar{N}_{200}^{D+2} + 8\bar{\zeta}_k^4 \bar{\mu}_k^3 \bar{N}_{200}^{D+2} - 12\bar{\zeta}_k^2 \bar{\lambda}_k \bar{\mu}_k \bar{N}_{100}^D \\
& \left. - 20\bar{\zeta}_k^2 \bar{\mu}_k^2 \bar{N}_{100}^D \right) \tag{A1}
\end{aligned}$$

where the threshold functions $\bar{L}_{abc}^{D+\alpha}$, $\bar{N}_{abc}^{D+\alpha}$ and $\bar{M}_{abc}^{D+\alpha}$ are given in the following section.

Appendix B: Threshold functions

Here we provide the expressions of the dimensionful and dimensionless threshold functions in D dimensions,

$$\begin{cases} L_{abc}^{D+\alpha} = -\frac{1}{4A_D} \hat{\partial}_t \int_q \mathbf{q}^\alpha (P(\mathbf{q}) + \mathbf{q}^2 m_0^2)^{-a} (P(\mathbf{q}) + \mathbf{q}^2 m_1^2)^{-b} (P(\mathbf{q}) + \mathbf{q}^2 m_2^2)^{-c} \\ N_{abc}^{D+\alpha} = -\frac{1}{4A_D} \hat{\partial}_t \int_q \mathbf{q}^\alpha \frac{\partial P(\mathbf{q})}{\partial \mathbf{q}^2} (P(\mathbf{q}) + \mathbf{q}^2 m_0^2)^{-a} (P(\mathbf{q}) + \mathbf{q}^2 m_1^2)^{-b} (P(\mathbf{q}) + \mathbf{q}^2 m_2^2)^{-c} \\ M_{abc}^{D+\alpha} = -\frac{1}{4A_D} \hat{\partial}_t \int_q \mathbf{q}^\alpha \left(\frac{\partial P(\mathbf{q})}{\partial \mathbf{q}^2} \right)^2 (P(\mathbf{q}) + \mathbf{q}^2 m_0^2)^{-a} (P(\mathbf{q}) + \mathbf{q}^2 m_1^2)^{-b} (P(\mathbf{q}) + \mathbf{q}^2 m_2^2)^{-c} \end{cases} \tag{B1}$$

with $A_D = 1/2^{D+1} \pi^{D/2} \Gamma(D/2)$, $P(\mathbf{q}) = Z_k \mathbf{q}^4 + R_k(\mathbf{q})$, $\hat{\partial}_t = \partial_t R_k(\mathbf{q}) \partial_{R_k}$.

Below we give the threshold functions $L_{a00}^{D+\alpha}$, $N_{a00}^{D+\alpha}$ and $M_{a00}^{D+\alpha}$ that are relevant to study the flat phase which is governed by massless flexurons modes. We thus put $m_0 = 0$. One has:

$$\begin{cases} L_{a00}^{D+\alpha} = -\frac{1}{4A_D} \hat{\partial}_t \int_q \mathbf{q}^\alpha P(\mathbf{q})^{-a} \\ N_{a00}^{D+\alpha} = -\frac{1}{4A_D} \hat{\partial}_t \int_q \mathbf{q}^\alpha \frac{\partial P(\mathbf{q})}{\partial \mathbf{q}^2} P(\mathbf{q})^{-a} \\ M_{a00}^{D+\alpha} = -\frac{1}{4A_D} \hat{\partial}_t \int_q \mathbf{q}^\alpha \left(\frac{\partial P(\mathbf{q})}{\partial \mathbf{q}^2} \right)^2 P(\mathbf{q})^{-a} \end{cases} \tag{B2}$$

with $\int_q = \int \frac{d^D q}{(2\pi)^D} := \int d^D q$ and $d^D q = 4A_D q^{D-1} dq$.

We now set $x = \mathbf{q}^2$ so that $d^D q = 2A_D x^{(D-2)/2} dx$

dimensions, the latter ones being used in practical computations to identify fixed points.

1. The monolayer case

a. Definitions

The thresholds functions involving three propagators thus with three pseudo-masses m_0 , m_1 and m_2 are defined as:

and apply $\hat{\partial}_t = \partial_t R_k(\mathbf{q}) \partial_{R_k}$. One gets:

$$\begin{cases} L_{a00}^{D+\alpha} = \frac{1}{2} \int dx x^{\frac{D+\alpha}{2}-1} \frac{a \partial_t R_k(x)}{(Z_k x^2 + R_k(x))^{a+1}} \\ N_{a00}^{D+\alpha} = -\frac{1}{2} \int dx x^{\frac{D+\alpha}{2}-1} \left[\frac{\partial_t \partial_x P(x)}{(Z_k x^2 + R_k(x))^a} \right. \\ \left. M_{a00}^{D+\alpha} = -\frac{1}{2} \int dx x^{\frac{D+\alpha}{2}-1} \left[\frac{2 \partial_x P(x) \partial_t \partial_x P(x)}{(Z_k x^2 + R_k(x))^a} \right. \right. \\ \left. \left. - \frac{a (\partial_x P(x))^2 \partial_t R_k(x)}{(Z_k x^2 + R_k(x))^{a+1}} \right] \right]. \end{cases} \tag{B3}$$

b. Dimensionless threshold functions

We now express the thresholds functions in terms dimensionless quantities. One writes:

$$R_k(\mathbf{q})[y] = Z_k k^4 y^2 r_k(y) \quad \text{with} \quad y = \frac{x}{k^2}, \tag{B4}$$

where $r_k(y)$ is the dimensionless cut-off function and y is a dimensionless variable. With this expression,

one can evaluate:

$$P(\mathbf{q})[y] = Z_k \mathbf{q}^4 + R_k(\mathbf{q}) = Z_k k^4 y^2 (1 + r_k(y)) \quad (\text{B5})$$

and compute all the quantities needed for the evaluations of the threshold functions Eq. (B3). One has:

$$\partial_t R_k(x)[y] = -Z_k k^4 [\eta_k y^2 r_k(y) + 2y^3 \partial_y r_k(y)] \quad (\text{B6})$$

$$\partial_x P(x)[y] = Z_k k^2 [2y(1 + r_k(y)) + y^2 \partial_y r_k(y)] \quad (\text{B7})$$

and

$$\begin{aligned} \widehat{\partial}_t \partial_y P(x)[y] &= \partial_y \widehat{\partial}_t P(x)[y] = \partial_y \partial_t R_k(x)[y] \\ &= -Z_k k^2 [2\eta_k y r_k(y) + y^2(\eta_k + 6) \partial_y r_k(y) \\ &\quad + 2y^3 \partial_y^2 r_k(y)] . \end{aligned} \quad (\text{B8})$$

This leads to the dimensionless threshold functions:

$$\left\{ \begin{array}{l} \bar{L}_{a00}^{D+\alpha} = -\frac{a}{2} \int dy y^{\frac{D+\alpha-2}{2}-2a} \left[\frac{\eta_k r_k(y) + 2y \partial_y r_k(y)}{(1+r_k(y))^{a+1}} \right] \\ \bar{N}_{a00}^{D+\alpha} = \frac{1}{2} \int dy y^{\frac{D+\alpha}{2}-2a} \left[\frac{2\eta_k r_k(y) + y(\eta_k + 6) \partial_y r_k(y) + 2y^2 \partial_y^2 r_k(y)}{(1+r_k(y))^a} \right. \\ \quad \left. - a(2(1+r_k(y)) + y \partial_y r_k(y)) \frac{\eta_k r_k(y) + 2y \partial_y r_k(y)}{(1+r_k(y))^{a+1}} \right] \\ \bar{M}_{a00}^{D+\alpha} = \frac{1}{2} \int dy y^{\frac{D+\alpha+2}{2}-2a} (2(1+r_k(y)) + y \partial_y r_k(y)) \left[\frac{2(2\eta_k r_k(y) + y(\eta_k + 6) \partial_y r_k(y) + 2y^2 \partial_y^2 r_k(y))}{(1+r_k(y))^a} \right. \\ \quad \left. - a(2(1+r_k(y)) + y \partial_y r_k(y)) \frac{\eta_k r_k(y) + 2y \partial_y r_k(y)}{(1+r_k(y))^{a+1}} \right] \end{array} \right. \quad (\text{B9})$$

while the dimensionful and dimensionless threshold functions are related by:

$$\begin{cases} L_{abc}^{2+\alpha} = (Z_k k^4)^{-a-b-c} k^{D+\alpha} \bar{L}_{abc}^{2+\alpha} \\ N_{abc}^{2+\alpha} = (Z_k k^4)^{-a-b-c} Z_k k^{D+2+\alpha} \bar{N}_{abc}^{2+\alpha} \\ M_{abc}^{2+\alpha} = (Z_k k^4)^{-a-b-c} Z_k^2 k^\alpha \bar{M}_{abc}^{D+4+\alpha} \end{cases} \quad (\text{B10})$$

$$\begin{cases} \bar{L}_{a00}^{D+\alpha} = \frac{4a}{D+\alpha} - \eta_k \frac{4a}{(D+\alpha)(D+4+\alpha)} \\ \bar{N}_{a00}^{D+\alpha} = 2 - \eta_k \frac{2}{D+2+\alpha} \\ \bar{M}_{a00}^{D+\alpha} = 4 . \end{cases} \quad (\text{B13})$$

where one has taken $\Theta(0) = 1/2$.

c. Litim (or Θ) cut-off

We have chosen to use the Litim cut-off as cut-off function $R_k(\mathbf{q})$:

$$R_k(\mathbf{q})[y] = Z_k (k^4 - |\mathbf{q}|^4) \Theta(k^2 - |\mathbf{q}|^2) = Z_k k^4 r_k(y) \quad (\text{B11})$$

with: $r_k(y) = \frac{1-y^{-2}}{y^2} \Theta(1-y^2)$.

We compute the derivatives:

$$\begin{cases} \partial_y r_k(y) = -2y^{-3} \Theta(1-y^2) \\ \partial_y^2 r_k(y) = 6y^{-4} \Theta(1-y^2) + 4y^{-3} \delta(1-y^2) . \end{cases} \quad (\text{B12})$$

We finally obtain the following form for the threshold functions:

2. The bilayer case

a. Definitions

In the case of bilayer membranes in the flat phase the relevant threshold functions are:

$$\begin{cases} {}^B L_{a00}^{D+\alpha} = -\frac{1}{4 A_D} \widehat{\partial}_t \int_q \mathbf{q}^\alpha P_{c_k}(\mathbf{q})^{-a} \\ {}^B N_{a00}^{D+\alpha} = -\frac{1}{4 A_D} \widehat{\partial}_t \int_q \mathbf{q}^\alpha \frac{\partial P_{c_k}(\mathbf{q})}{\partial \mathbf{q}^2} P_{c_k}(\mathbf{q})^{-a} \end{cases} \quad (\text{B14})$$

with $P_{c_k}(\mathbf{q}) = \left(Z_k + \ell_k^2 \frac{\lambda_k^2 + 2\mu_k^2}{4} \right) \mathbf{q}^4 + R_k(\mathbf{q})$.

b. Dimensionless threshold functions

Proceeding in the same way as in the monolayer case, one obtains for the dimensionless threshold functions:

$$\left\{ \begin{array}{l} {}^B\bar{L}_{a00}^{D+\alpha} = -\frac{a}{2} \int dy y^{\frac{D+\alpha-2}{2}-2a} \left[\frac{\eta_k r_k(y) + 2y \partial_y r_k(y)}{(1+\bar{c}_k + r_k(y))^{a+1}} \right] \\ {}^B\bar{N}_{a00}^{D+\alpha} = \frac{1}{2} \int dy y^{\frac{D+\alpha}{2}-2a} \left[\frac{2\eta_k r_k(y) + y(\eta_k + 6) \partial_y r_k(y) + 2y^2 \partial_y^2 r_k(y)}{(1+\bar{c}_k + r_k(y))^a} \right. \\ \left. - a(2(1+r_k(y)+\bar{c}_k) + y \partial_y r_k(y)) \frac{\eta_k r_k(y) + 2y \partial_y r_k(y)}{(1+\bar{c}_k + r_k(y))^{a+1}} \right] \end{array} \right. \quad (B15)$$

with $\bar{c}_k = \bar{\ell}_k^2 \frac{\bar{\lambda}_k + 2\bar{\mu}_k}{4}$.

c. Litim cut-off

Using then the Litim cut-off one gets:

$$\left\{ \begin{array}{l} {}^B\bar{L}_{a00}^{D+\alpha} = a(4-\eta_k) \frac{2F_1(1+a, \frac{D+\alpha}{4}, \frac{D+\alpha+4}{4}, -\bar{c}_k)}{D+\alpha} \\ + a\eta_k \frac{2F_1(1+a, \frac{D+\alpha+4}{4}, \frac{D+\alpha+8}{4}, -\bar{c}_k)}{D+\alpha+4} \\ {}^B\bar{N}_{a00}^{D+\alpha} = \frac{2}{(1+\bar{c}_k)^a} \\ - 2\eta_k \frac{2F_1(a, \frac{D+\alpha+2}{4}, \frac{D+\alpha+6}{4}, -\bar{c}_k)}{D+\alpha+2} \\ - 2a\bar{c}_k(\eta_k-4) \frac{2F_1(1+a, \frac{D+\alpha+2}{4}, \frac{D+\alpha+6}{4}, -\bar{c}_k)}{D+\alpha+2} \\ + 2a\bar{c}_k \eta_k \frac{2F_1(1+a, \frac{D+\alpha+6}{4}, \frac{D+\alpha+10}{4}, -\bar{c}_k)}{D+\alpha+6} \end{array} \right. \quad (B16)$$

Appendix C: Propagators of bilayer membranes

We give here the expressions of the full propagators:

$$\left\{ \begin{array}{l} G_{k,1rr}(\mathbf{q}) = \frac{1}{2(Z_k \mathbf{q}^4 + \mathbf{q}^2 \zeta_k^2 \mu_k + R_k(\mathbf{q}))}, \\ G_{k,2rr}(\mathbf{q}) = \frac{1}{2(Z_k \mathbf{q}^4 + \mathbf{q}^2 \zeta_k^2 (\lambda + 2\mu_k) + R_k(\mathbf{q}))} \\ G_{k,1rs}(\mathbf{q}) = \frac{2}{Z_k \mathbf{q}^4 + \zeta_k^2 (2g_{2k}/\ell_k^2 + \mathbf{q}^2 \mu_k) + R_k(\mathbf{q})}, \\ G_{k,2rs}(\mathbf{q}) = \frac{4\ell_k^2}{2g_{2k}(\lambda_k^2 \mathbf{q}^2 + \zeta_k^2) + \ell_k^2 (5Z_k \mathbf{q}^4 + \mathbf{q}^2 \zeta_k^2 (\lambda_k + 2\mu_k) + 5R_k(\mathbf{q})) + \sqrt{\Delta}}, \\ G_{k,3rs}(\mathbf{q}) = \frac{4\ell_k^2}{2g_{2k}(\ell_k^2 \mathbf{q}^2 + \zeta_k^2) + \ell_k^2 (5Z_k \mathbf{q}^4 + \mathbf{q}^2 \zeta_k^2 (\lambda_k + 2\mu_k) + 5R_k(\mathbf{q})) - \sqrt{\Delta}} \\ G_{k,ss}(\mathbf{q}) = \frac{2}{Z_k \mathbf{q}^4 + 2g_{1k}/\ell_k^2 + R_k(\mathbf{q})} \end{array} \right. \quad (C1)$$

with

$$\begin{aligned} \Delta = & 4g_{2k}^2(\ell_k^2 \mathbf{q}^2 + \zeta_k^2)^2 + 4g_{2k}\ell_k^2 \mathbf{q}^2 (\ell_k^2 \mathbf{q}^2 - \zeta_k^2) \left(3Z_k \mathbf{q}^2 - \zeta_k^2 (\lambda_k + 2\mu_k) \right) + \ell_k^4 \mathbf{q}^4 \left(3Z_k \mathbf{q}^2 - \zeta_k^2 (\lambda_k + 2\mu_k) \right)^2 \\ & + 3\ell_k^2 R_k(\mathbf{q}) \left(4g_{2k}(\ell_k^2 \mathbf{q} - \zeta_k^2) + 2\ell_k^2 \mathbf{q}^2 (3Z_k \mathbf{q}^2 - \zeta_k^2 (\lambda_k + 2\mu_k)) + 3\ell_k^2 R_k(\mathbf{q}) \right). \end{aligned} \quad (C2)$$

Appendix D: Geometry of the bilayer: parallel surfaces

We give here the expression for the induced metric on (Σ_d) , the hypersurface obtained by translating a hypersurface (Σ) by a (signed) distance d along its unit normal in \mathbb{R}^3 .

We describe the mean surface of the bilayer as an embedding

$$\mathbf{r}(x^1, x^2) \in \mathbb{R}^3, \quad (D1)$$

with local coordinates x^α ($\alpha = 1, 2$).

a. Tangent basis, metric, normal and curvature.
The tangent vectors are

$$\mathbf{e}_\alpha = \partial_\alpha \mathbf{r}, \quad (D2)$$

and the induced (first fundamental) metric is

$$g_{\alpha\beta} = \mathbf{e}_\alpha \cdot \mathbf{e}_\beta. \quad (D3)$$

We choose a unit normal field \mathbf{n} such that

$$\mathbf{n} \cdot \mathbf{e}_\alpha = 0, \quad \mathbf{n} \cdot \mathbf{n} = 1. \quad (D4)$$

The second fundamental form (curvature tensor) is defined as

$$K_{\alpha\beta} = \mathbf{n} \cdot \partial_\alpha \partial_\beta \mathbf{r}. \quad (D5)$$

It is convenient to introduce the mixed tensor (shape operator)

$$K_\alpha^\gamma = g^{\gamma\delta} K_{\alpha\delta}, \quad (\text{D6})$$

with $g^{\alpha\beta}$ the inverse of $g_{\alpha\beta}$. The Weingarten relation expresses the derivative of the normal in the tangent basis:

$$\partial_\alpha \mathbf{n} = -K_\alpha^\gamma \mathbf{e}_\gamma. \quad (\text{D7})$$

b. *Parallel surfaces at signed distance d .* We now consider the surface obtained by shifting \mathbf{r} a signed distance d along the normal:

$$\mathbf{r}_d(x) = \mathbf{r}(x) + d \mathbf{n}(x). \quad (\text{D8})$$

Its tangent vectors are

$$\partial_\alpha \mathbf{r}_d = \partial_\alpha \mathbf{r} + d \partial_\alpha \mathbf{n} = \mathbf{e}_\alpha + d \partial_\alpha \mathbf{n}. \quad (\text{D9})$$

Using the Weingarten relation,

$$\partial_\alpha \mathbf{n} = -K_\alpha^\gamma \mathbf{e}_\gamma, \quad (\text{D10})$$

we find

$$\partial_\alpha \mathbf{r}_d = \mathbf{e}_\alpha - d K_\alpha^\gamma \mathbf{e}_\gamma. \quad (\text{D11})$$

The induced metric on the shifted surface is

$$g_{\alpha\beta}(d) = \partial_\alpha \mathbf{r}_d \cdot \partial_\beta \mathbf{r}_d. \quad (\text{D12})$$

Inserting the expression for $\partial_\alpha \mathbf{r}_d$,

$$\begin{aligned} g_{\alpha\beta}(d) &= (\mathbf{e}_\alpha - d K_\alpha^\gamma \mathbf{e}_\gamma) \cdot (\mathbf{e}_\beta - d K_\beta^\delta \mathbf{e}_\delta) \\ &= \mathbf{e}_\alpha \cdot \mathbf{e}_\beta - d K_\alpha^\gamma (\mathbf{e}_\gamma \cdot \mathbf{e}_\beta) - d K_\beta^\delta (\mathbf{e}_\alpha \cdot \mathbf{e}_\delta) \\ &\quad + d^2 K_\alpha^\gamma K_\beta^\delta (\mathbf{e}_\gamma \cdot \mathbf{e}_\delta). \end{aligned}$$

Using $\mathbf{e}_\gamma \cdot \mathbf{e}_\beta = g_{\gamma\beta}$, this becomes

$$g_{\alpha\beta}(d) = g_{\alpha\beta} - d K_\alpha^\gamma g_{\gamma\beta} - d K_\beta^\delta g_{\alpha\delta} + d^2 K_\alpha^\gamma K_\beta^\delta g_{\gamma\delta}.$$

The linear terms simplify using

$$K_{\alpha\beta} = \mathbf{n} \cdot \partial_\alpha \partial_\beta \mathbf{r} = g_{\beta\gamma} K_\alpha^\gamma, \quad (\text{D13})$$

and the symmetry $K_{\alpha\beta} = K_{\beta\alpha}$, which implies

$$K_\alpha^\gamma g_{\gamma\beta} = K_{\alpha\beta}, \quad K_\beta^\delta g_{\alpha\delta} = K_{\beta\alpha} = K_{\alpha\beta}. \quad (\text{D14})$$

Hence the linear part in d is $-2d K_{\alpha\beta}$. The quadratic part can be written as

$$(K^2)_{\alpha\beta} = K_\alpha^\gamma b_{\gamma\beta}. \quad (\text{D15})$$

Altogether we obtain the standard formula for the metric of a parallel surface:

$$g_{\alpha\beta}(d) = g_{\alpha\beta} - 2d K_{\alpha\beta} + d^2 (K^2)_{\alpha\beta}. \quad (\text{D16})$$

[1] K. S. Novoselov, A. K. Geim, S. V. Morozov, D. Jiang, Y. Zhang, S. V. Dubonos, I. V. Grigorieva, and A. A. Firsov, *Science* **306**, 666 (2004).

[2] K. S. Novoselov, A. K. Geim, S. V. Morozov, D. Jiang, M. I. Katsnelson, I. V. Grigorieva, S. V. Dubonos, and A. A. Firsov, *Nature (London)* **438**, 197 (2005).

[3] M. I. Katsnelson, *Graphene: Carbon in Two Dimensions* (Cambridge University Press, Cambridge, U.K., 2012).

[4] D. Akinwande, C. J. Brennan, J. Scott Bunch, P. Egberts, J. R. Felts, H. Gao, R. Huang, J.S. Kim, T. Li, Y. Li, K. M. Liechti, N. Lu, H.S. Park, E. J. Reed, P. Wang, B.I. Yakobson, T. Zhang, Y.W. Zhang, Y. Zhou and Y. Zhu, *Extreme Mech. Lett.* **13**, 42 (2017).

[5] A. H. Castro Neto, F. Guinea, N. M. R. Peres, K. S. Novoselov, and A. K. Geim, *Rev. Mod. Phys.* **81**, 109 (2009).

[6] Z. Gao *et al.*, *J.Phys. Mater.* **3**, 042003 (2020).

[7] A. Nimbalkar and H. Kim, *Nano-Micro Lett.* **12**, 126 (2020).

[8] P.A. Pantaleón, A. Jimeno-Pozo, H. Sainz-Cruz, V. Tié Phong, T. Cea and F. Guinea, *Nat. Rev. Phys.* **5**, 304 (2023).

[9] E. McCann and M. Koshino, *Rep. Prog. Phys.* **76**, 056503 (2013).

[10] A. V. Rozhkov, A. O. Sboychakov, A. L. Rakhmanov, and F. Nori, *Phys. Rep.* **648**, 1 (2016).

[11] E.Y. Andrei and A.H. MacDonald, *Nat. Mater.* **19**, 1265 (2020).

[12] Y. Chu, F. Zhu, L. Wen, W. Chen, Q. Chen, and T. Ma, *Chin. Phys. B* **29**, 117401 (2020).

[13] M.J. Calderón and E. Bascones, *npj Quantum Mater.* **5**, 57 (2020).

[14] D. R. Nelson, T. Piran, and S. Weinberg, eds., *Statistical Mechanics of Membranes and Surfaces*, 2nd ed. (World Scientific Publishing, Singapore, 2004) paperback ISBN: 978-981-238-772-1.

[15] A. Fasolino, J. Los, and M. Katsnelson, *Nat. Mater.* **6**, 858 (2007).

[16] M. Katsnelson and A. Fasolino, *Acc. Chem. Res.* **46**, 97 (2013).

[17] J. H. Los, A. Fasolino, and M. I. Katsnelson, *npj 2D Materials and Applications* **1**, 31 (2017).

[18] D. R. Nelson and L. Peliti, *J. Phys. (Paris)* **48**, 1085 (1987).

[19] J. A. Aronovitz, L. Golubovic, and T. C. Lubensky, *J. Phys. (Paris)* **50**, 609 (1989).

[20] O. Coquand, *Phys. Rev B* **100**, 125406 (2019).

[21] N. D. Mermin and H. Wagner, *Phys. Rev. Lett.* **17**, 1133 (1966).

[22] P. Hohenberg, *Phys. Rev.* **158**, 383 (1967).

[23] J. A. Aronovitz and T. C. Lubensky, *Phys. Rev. Lett.* **60**, 2634 (1988).

[24] F. David and E. Guitter, *Europhys. Lett.* **5**, 709 (1988).

[25] E. Guitter, F. David, S. Leibler, and L. Peliti, *Phys. Rev. Lett.* **61**, 2949 (1988).

[26] E. Guitter, F. David, S. Leibler, and L. Peliti, *J. Phys. (Paris)* **50**, 1787 (1989).

[27] P. Le Doussal and L. Radzihovsky, *Phys. Rev. Lett.* **69**, 1209 (1992).

[28] K. V. Zakharchenko, R. Roldán, A. Fasolino and M.

I. Katsnelson, *Phys. Rev. B* **82**, 125435 (2010).

[29] R. Roldán, A. Fasolino, K. V. Zakharchenko, and M. I. Katsnelson, *Phys. Rev. B* **83**, 174104 (2011).

[30] P. Le Doussal and L. Radzihovsky, *Ann. Phys. (Amsterdam)* **392**, 340 (2018).

[31] D. Gazit, *Phys. Rev. E* **80**, 041117 (2009).

[32] Z. Zhang, H. T. Davis, and D. M. Kroll, *Phys. Rev. E* **48**, R651 (1993).

[33] M. J. Bowick and S. Catterall and M. Falcioni and G. Thorleifsson and K. Anagnostopoulos., *J. Phys. I (France)* **6**, 1321 (1996).

[34] A. Tröster, *Phys. Rev. B* **87**, 104112 (2013).

[35] O. Coquand, D. Mouhanna, and S. Teber, *Phys. Rev. E* **101**, 062104 (2020).

[36] S. Metayer, D. Mouhanna, and S. Teber, *Phys. Rev. E* **105**, L012603 (2022).

[37] S. Metayer and D. Mouhanna, *Phys. Rev. E* **106**, 064114 (2022).

[38] S. Metayer, D. Mouhanna and S. Teber, *J. Phys. Conf. Ser.* **2438**, 012141 (2023).

[39] A. Pikelner, *Europhys. Lett.* **138**, 17002 (2022).

[40] J.-P. Kownacki and D. Mouhanna, *Phys. Rev. E* **79**, 040101(R) (2009).

[41] F. L. Braghin and N. Hasselmann, *Phys. Rev. B* **82**, 035407 (2010).

[42] N. Hasselmann and F. L. Braghin, *Phys. Rev. E* **83**, 031137 (2011).

[43] K. Essafi, J.-P. Kownacki, and D. Mouhanna, *Phys. Rev. E* **89**, 042101 (2014).

[44] J. H. Los, M. I. Katsnelson, O. Y. Yazyev, K. V. Zarharchenko, and A. Fasolino, *Phys. Rev. B* **80**, 121405(R) (2009).

[45] A. Mauri, D. Soriano and M.I. Katsnelson, *Phys. Phys. B* **102**, 165421 (2020).

[46] N. Lindahl, D. Midtvedt, J. Svenson, O. A. Nerushev, N. Lindvall, A. Isacsson and E. Campbell, *Nano Lett.* **12**, 3526 (2012).

[47] B. Sajadi, S. van Hemert, B. Arash, P. Belardinelli, P. G. Steeneken, and F. Alijani, *Carbon* **139**, 334 (2018).

[48] S. D. Eder, M. Tømterud, S. K. Hellner, L. Bignardi, P. Lacovig, S. Lizzit, C. Colletti, J. R. Manson, and B. Holst, *Phys. Rev. Lett.* **127**, 266102 (2021).

[49] C. P. Herrero and R. Ramírez, *Eur. Phys. J. B* **96**, 147 (2023).

[50] E. Han, J. Yu, E. Annevelink, J. Son, D. A. Kang, K. Watanabe, T. Taniguchi, E. Ertekin, P. Y. Huang, and A. M. van der Zande, *Nat. Mater.* **19**, 305 (2020).

[51] Y. Yang, S. Sridhar, Z. Liu, D. Wang, H. Zhou, J. Deng, H. Beng Chew and C. Ke, *Applied Physics Letters* **122**, 153101 (2023).

[52] P.L. de Andres, F. Guinea and M.I. Katsnelson, *Phys. Rev. B* **86**, 144103 (2012).

[53] M. Paczuski, M. Kardar, and D. R. Nelson, *Phys. Rev. Lett.* **60**, 2638 (1988).

[54] M. Paczuski and M. Kardar, *Phys. Rev. A* **39**, 6086 (1989).

[55] A. Mauri and M.I. Katsnelson, *Nucl. Phys. B* **956**, 115040 (2020).

[56] C. Wetterich, *Z. Phys. C* **57**, 451 (1993).

[57] N. Tetradis and C. Wetterich, *Nucl. Phys. B [FS]* **422**, 541 (1994).

[58] J. Berges, N. Tetradis, and C. Wetterich, *Phys. Rep.* **363**, 223 (2002).

[59] J. Pawłowski, *Ann. Phys. (N.Y.)* **322**, 2831 (2007).

[60] B. Delamotte, *Lect. Notes Phys.* **852**, 49 (2012).

[61] N. Dupuis, L. Canet, A. Eichhorn, W. Metzner, J. M. Pawłowski, M. Tissier, N. Wschebor, *Physics Reports* **1**, 910 (2021).

[62] K. G. Wilson and J. Kogut, *Phys. Rep.*, *Phys. Lett. 12C*, 75 (1974).

[63] C. Wetterich, *Phys. Lett. B* **301**, 90 (1993).

[64] T. R. Morris, *Int. J. Mod. Phys. A* **9**, 2411 (1994).

[65] D. Litim, *Phys. Rev. D* **64**, 105007 (2001).

[66] G. Tarjus and M. Tissier, *Eur. Phys. J. B* **93**, 50 (2020).

[67] In a standard scalar theory, massive terms are those with fewer than two derivatives compared to the kinetic term, which behaves as $(\partial\phi)^2$. In membrane theory, the kinetic term behaves as $(\partial^2 r)^2$. Thus, by analogy, the terms proportional to $(\partial r)^2$ are referred to as having a “pseudo-mass”.

[68] K. Essafi, J.-P. Kownacki and D. Mouhanna, *Phys. Rev. Lett.* **106**, 128102 (2011).

[69] O. Coquand and D. Mouhanna, *Phys. Rev. E* **94**, 032125 (2016).

[70] O. Coquand, K. Essafi, J.-P. Kownacki, and D. Mouhanna, *Phys. Rev E* **97**, 030102(R) (2018).

[71] D. Litim, *Int. J. Mod. Phys. A* **16**, 2081 (2001).

[72] L. Canet, B. Delamotte, D. Mouhanna, and J. Vidal, *Phys. Rev. D* **67**, 065004 (2003).